



Subcellular Localization of HIV-1 *gag-pol* mRNAs Regulates Sites of Virion Assembly

Jordan T. Becker, Nathan M. Sherer

McArdle Laboratory for Cancer Research, Institute for Molecular Virology, and Carbone Cancer Center, University of Wisconsin—Madison, Madison, Wisconsin, USA

ABSTRACT Full-length unspliced human immunodeficiency virus type 1 (HIV-1) RNAs serve dual roles in the cytoplasm as mRNAs encoding the Gag and Gag-Pol capsid proteins as well as genomic RNAs (gRNAs) packaged by Gag into virions undergoing assembly at the plasma membrane (PM). Because Gag is sufficient to drive the assembly of virus-like particles even in the absence of gRNA binding, whether viral RNA trafficking plays an active role in the native assembly pathway is unknown. In this study, we tested the effects of modulating the cytoplasmic abundance or distribution of full-length viral RNAs on Gag trafficking and assembly in the context of single cells. Increasing full-length viral RNA abundance or distribution had little-to-no net effect on Gag assembly competency when provided in *trans*. In contrast, artificially tethering full-length viral RNAs or surrogate *gag-pol* mRNAs competent for Gag synthesis to non-PM membranes or the actin cytoskeleton severely reduced net virus particle production. These effects were explained, in large part, by RNA-directed changes to Gag's distribution in the cytoplasm, yielding aberrant subcellular sites of virion assembly. Interestingly, RNA-dependent disruption of Gag trafficking required either of two *cis*-acting RNA regulatory elements: the 5' packaging signal (Psi) bound by Gag during genome encapsidation or, unexpectedly, the Rev response element (RRE), which regulates the nuclear export of gRNAs and other intron-retaining viral RNAs. Taken together, these data support a model for native infection wherein structural features of the *gag-pol* mRNA actively compartmentalize Gag to preferred sites within the cytoplasm and/or PM.

IMPORTANCE The spatial distribution of viral mRNAs within the cytoplasm can be a crucial determinant of efficient translation and successful virion production. Here we provide direct evidence that mRNA subcellular trafficking plays an important role in regulating the assembly of human immunodeficiency virus type 1 (HIV-1) virus particles at the plasma membrane (PM). Artificially tethering viral mRNAs encoding Gag capsid proteins (*gag-pol* mRNAs) to distinct non-PM subcellular locales, such as cytoplasmic vesicles or the actin cytoskeleton, markedly alters Gag subcellular distribution, relocates sites of assembly, and reduces net virus particle production. These observations support a model for native HIV-1 assembly wherein HIV-1 *gag-pol* mRNA localization helps to confine interactions between Gag, viral RNAs, and host determinants in order to ensure virion production at the right place and right time. Direct perturbation of HIV-1 mRNA subcellular localization may represent a novel antiviral strategy.

KEYWORDS Gag, MS2, packaging, Psi, RNA trafficking, RRE, genomes, human immunodeficiency virus, translation, virus assembly

The spatial distribution of mRNAs within the cytoplasm is a core determinant of mRNA turnover, cytoplasmic utilization, and the formation of functional macromolecular complexes (1–3). Viruses face severe challenges in this regard during the productive phases of infection, during which viral mRNAs, genomes, and core structural

Received 30 November 2016 Accepted 23 December 2016

Accepted manuscript posted online 4 January 2017

Citation Becker JT, Sherer NM. 2017. Subcellular localization of HIV-1 *gag-pol* mRNAs regulates sites of virion assembly. J Virol 91:e02315-16. <https://doi.org/10.1128/JVI.02315-16>.

Editor Frank Kirchhoff, Ulm University Medical Center

Copyright © 2017 American Society for Microbiology. All Rights Reserved.

Address correspondence to Nathan M. Sherer, nsherer@wisc.edu.

elements must be successfully compartmentalized in space and time to ensure the efficient assembly and release of infectious virions (4–6).

For the retrovirus human immunodeficiency virus type 1 (HIV-1), virion assembly is coordinated at the cytoplasmic face of the plasma membrane (PM), where a dimer of ~9 kb of unspliced genomic RNA (gRNA) is encapsidated into an enveloped, proteinaceous shell consisting of ~2,000 Gag (and Gag-Pol) capsid polyproteins (7, 8). To initiate assembly, Gag interacts with the PM via a fatty acid myristoyl membrane anchor and must also interact with an RNA scaffold in the cytoplasm (9–13). Four functional domains of the 55-kDa Gag precursor polyprotein ($\text{Pr}55^{\text{Gag}}$) coordinate this process. Matrix (MA/p17^{Gag}) targets Gag to the cytosolic face of the PM through interactions with the phospholipid phosphatidylinositol 4,5-bisphosphate [$\text{PI}(4,5)\text{P}_2$] (14–16). Capsid (CA/p24^{Gag}) coordinates Gag-Gag interactions during capsid assembly (7, 17–19). Nucleocapsid (NC/p7^{Gag}) binds to gRNAs and/or cellular RNAs (20–24). The late domain (p6^{Gag}) recruits the cellular endosomal sorting complex required for transport (ESCRT) machinery, which catalyzes membrane abscission and particle release (25–28).

A single cytoplasmic pool of HIV-1 full-length RNA molecules is thought to serve as the source of both mRNAs encoding Gag and Gag-Pol and the core genetic substrate (gRNAs) bound by Gag and packaged into virions (29–33). Herein we refer to either full-length species regardless of its activity as a gRNA for simplicity. How gRNAs are differentially programmed for translation versus packaging is not yet fully elucidated but is thought to involve spatially and temporally regulated posttranscriptional modifications in conjunction with changes to the RNA secondary structure (22, 30, 33–37). Gag is translated on free polysomes either prior to or coincident with the formation of viral ribonucleoprotein (vRNP)-trafficking granules that consist of low-order multiples of Gag bound to gRNAs in conjunction with cellular RNA binding proteins (38). Recent advanced-imaging studies have demonstrated that VRNPs diffuse in the cytoplasm prior to being tethered to the PM by Gag (13, 39, 40). Assembly is initiated when cytoplasmic Gag concentrations reach a critical level, known as the cooperative threshold (41–43), triggering the activation of a myristoyl switch mechanism within MA that subsequently anchors genomic RNP (gRNP) complexes to the PM (12, 44, 45).

Gag selectively encapsidates a single dimer of gRNA molecules with high efficiency (46–49) due to the NC domain's capacity to bind a *cis*-acting RNA-packaging signal known as *Psi*, located in the gRNA's 5' untranslated region (UTR) with high affinity (21, 31, 33, 34, 50–52). A second *cis*-acting RNA structure, the Rev response element (RRE), may also contribute to gRNA encapsidation, albeit through an unknown mechanism (53, 54). However, the RRE is better characterized as regulating gRNA nucleocytoplasmic transport through recruitment of the viral Rev protein and subsequent Rev-mediated interactions with the cellular CRM1 nuclear export receptor (55–57). The dimerization of gRNAs may occur in the cytoplasm (58) and/or during Gag-PM anchoring (59), followed by the recruitment of additional Gag molecules to form an immature capsid lattice over a time period of 10 to 60 min (13, 40, 48, 60, 61). NC also binds to and packages cellular RNAs, with highly structured RNAs, such as U6 snRNAs, and 7SL RNAs encapsidated into virions with a high degree of specificity (23, 24, 49, 62, 63). The MA domain has also been reported to bind RNAs, in particular cellular tRNAs, an activity that regulates MA-membrane interactions *in vitro* and is thus predicted to impact assembly efficiency in cells (51, 64, 65).

Gag is sufficient to drive the assembly of noninfectious virus-like particles (VLPs) even in the absence of packageable gRNAs (66–71), and the rates of VLP assembly are roughly equivalent in the presence and absence of Psi-containing gRNAs (13). Thus, capsid-genome interactions are clearly not obligatory for HIV-1 assembly, unlike for many other viruses (72–74). On the other hand, imaging studies have demonstrated that gRNAs typically accumulate at the membrane prior to the onset of high-order Gag assembly, so that the gRNA may play a role in nucleating this process (13, 40). Moreover, we and others have demonstrated that manipulating gRNA trafficking (e.g., by rendering gRNAs or surrogate *gag-pol* mRNAs Rev/RRE independent) can, in some instances, profoundly affect Gag's capacity to traffic to the PM (75–80). An attractive,

long-standing hypothesis for links between HIV-1 mRNA trafficking and assembly is that, under native conditions, gRNAs encode one or more signals that influence gRNA/Gag subcellular distribution in the cytoplasm (75, 76, 79, 81). However, direct evidence for such an activity remains elusive.

In the current study, we combined imaging and functional assays to determine whether modulating the cytoplasmic abundance or physically perturbing the subcellular localization of gRNAs can either positively or negatively impact the assembly pathway. We observed that increasing the cytoplasmic abundance of gRNA with a disrupted *gag* coding sequence had little-to-no effect on Gag assembly when *gag* was expressed in *trans*. In contrast, disrupting gRNA diffusion in the cytoplasm by artificially tethering gRNAs to non-PM membranes or the actin cytoskeleton markedly affected Gag subcellular distribution and potently reduced virus particle production/release. Interestingly, these tethering effects were observed only for gRNAs competent for Gag synthesis (i.e., *gag-pol* mRNAs) and mapped to the 5' *Psi* element bound by Gag as well as the RRE, which governs gRNA nuclear export. Taken together, our results are consistent with a model wherein, under native conditions, Gag translation, gRNA trafficking, and Gag-gRNA interactions are compartmentalized in the cytoplasm and/or at the PM to promote efficient assembly.

RESULTS

Tracking Gag-gRNA interactions in single living cells. We first sought to determine if HIV-1 gRNAs encode trafficking activities that affect assembly efficiency when provided to Gag in *trans*. To this end, we coexpressed full-length gRNA transcripts with functional versions of codon-optimized Gag fused to a fluorescent protein (COGagFP); the *gag* coding region was codon optimized in order to achieve GagFP synthesis in the absence of Rev or any other viral factors (82, 83) (Fig. 1A and B, lane 5). To monitor both COGagFP and gRNA transcripts simultaneously, we inserted 24 copies of the MS2 bacteriophage RNA stem-loop (MS2 stem-loops [MSL]), recognized by the MS2 coat protein, between the *gag* and *pol* open reading frames within the major intron of a full-length wild-type HIV-1 subtype NL4-3-based luciferase reporter virus construct (WT-MSL) (Fig. 1). These gRNAs retained the capacity to express full-length, unlabeled Gag and yielded robust production of virus-like particles (VLPs) released from cells into the supernatant. Due to the insertion of the MSL cassette upstream of the *pol* gene, however, synthesis of the viral protease was abrogated such that the 55-kDa form of Gag was not cleaved to the 24-kDa form found in WT NL4-3 VLPs (Fig. 1A and B, lane 2). Both COGagFP and MSL-bearing gRNAs could be directly visualized in HeLa cells engineered to stably express the MS2-yellow fluorescent protein (YFP) fused to a carboxy-terminal nuclear localization signal (NLS) (HeLa.MS2-YFP) (Fig. 1C). In these cells, low levels of MS2-YFP are sequestered in the nucleus until bound to an MSL-containing gRNA and exported to the cytoplasm (Fig. 1C).

Investigating the effect of gRNAs on Gag trafficking in *trans* was confounded by the gRNA's essential role as the *gag/gag-pol* mRNA (76). Thus, we also generated constructs bearing a single nucleotide substitution (AUG→ACG) at the initiator methionine codon of Gag (1ACG-MSL, depicted in Fig. 1A). This mutation converts a wobble G-U base pair in the stem to a Watson-Crick G-C base pair and was chosen based on earlier predictions that it stabilizes RNA secondary structures conducive to the formation of functional Gag-gRNA complexes (52, 84). To control for cytoplasmic activities, we mutated 1ACG-MSL transcripts further by deleting the Rev response element (RRE), thus generating a gRNA incapable of exiting the nucleus due to the inability of HIV-1 Rev to facilitate CRM1-dependent gRNA nucleocytoplasmonic trafficking (dRRE-MSL) (Fig. 1A). As expected, neither 1ACG nor dRRE transcripts were competent for the translation of full-length Gag proteins (in Fig. 1B, compare lanes 3 and 4 to lane 2). However, 1ACG transcripts were both exported from the nucleus (Fig. 1C) and translated, as evidenced by low levels of a minor Gag isoform (p40) previously shown to result from initiation at *gag* codon methionine-142 (Fig. 1B, lane 3) but incapable of assembling particles on its own (85, 86). As expected, expression of WT-MSL and 1ACG-MSL gRNAs yielded

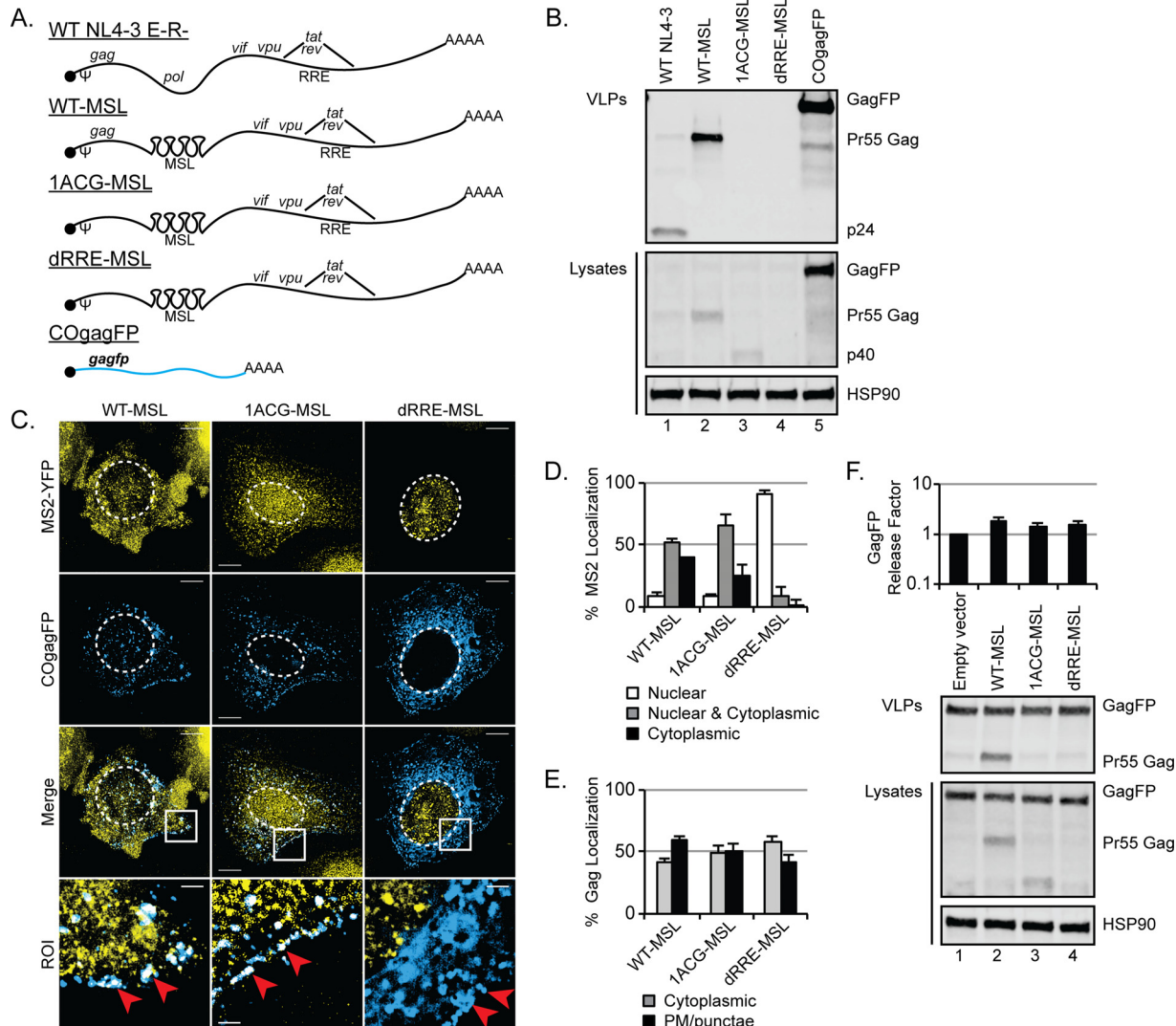


FIG 1 Tracking Gag-gRNA interactions in single living cells. (A) Cartoon depiction of gRNAs used in these studies. Ψ , Psi packaging signal; MSL, 24 copies of MS2 RNA stem-loop; RRE, Rev response element. *tat* and *rev* encode gene-regulatory proteins translated from completely spliced mRNAs. *vif* and *vpu* encode immune-modulatory proteins translated from partially spliced mRNAs. (B) HEK293T cells were transfected with 2,000 ng HIV-1 plasmids encoding the WT, modified, and mutated gRNAs depicted in panel A. VLPs and cell lysates were collected 48 h posttransfection, resolved by SDS-PAGE, and detected by immunoblotting using anti-p24^{Gag} antiserum (HSP90 was also detected as a loading control). (C) Widefield deconvolution microscopy images of HeLa.MS2-YFP cells transfected with 100 ng COGagFP and 900 ng HIV constructs. Cells were fixed \sim 30 h posttransfection and imaged. Single Z-plane images are shown. Scale bars represent 10 μ m in full images and 2 μ m in regions of interest (ROI). Dashed white lines show the relative positions of cell nuclei. The white boxes outline the ROI. Red arrows indicate sites where COGagFP has accumulated in PM-adjacent punctae. (D) Quantification of MS2-YFP localization phenotypes. Bar graphs show percentages of cells transfected with nuclear gRNA, cytoplasmic gRNA, or both distributions of gRNA for each transfection condition. (E) Quantification of GagFP distribution phenotypes. Bar graphs show percentages of cells transfected with diffuse or PM-adjacent punctae located in Gag for each transfection condition. (D and E) Error bars represent standard deviations from the means from at least four independent experiments quantifying at least 100 cells per condition. (F) HEK293T cells were cotransfected with 500 ng COGagFP and 1,500 ng of HIV gRNA constructs (as indicated) or an empty vector control (pBluescript) and immunoblotted as described for panel A. Bar graphs show fold change in Gag release factor (\log_{10} scale) from the empty-vector condition. The release factor is calculated from Gag band intensities in VLPs divided by lysates normalized to HSP90 ($n = 4$).

translocation of MS2-YFP from the nucleus to the cytoplasm in >50% of transfected HeLa.MS2-YFP cells at \sim 24 h posttransfection (Fig. 1C, and see the quantification in Fig. 1D). In contrast, dRRE-MSL gRNAs formed discrete MS2-YFP punctae that were retained in the nucleus in >90% of transfected cells, which is consistent with gRNA transcription events in the absence of nuclear export (Fig. 1C and D).

When coexpressed, WT- or 1ACG-gRNAs colocalized with COGagFP aggregates at the plasma membrane, consistent with Gag/gRNA cotrafficking to assembly sites (Fig. 1C, bottom panels). However, for each of these conditions, we observed only minor

differences in the frequencies of cells exhibiting PM-adjacent COGagFP aggregates (Fig. 1C, middle panels, and see the quantification in Fig. 1E). Moreover, COGagFP was released from cells with similar efficiencies when it was coexpressed with either 1ACG- or dRRE-gRNAs in a VLP assembly assay using HEK293T cells (Fig. 1F). These experiments demonstrated that at relatively high levels of Gag expression, COGagFP trafficking and assembly were only moderately affected by gRNA constructs expressed in *trans*, whether or not they generated gRNA transcripts competent for export into the cytoplasm.

Increasing HIV-1 gRNA cytoplasmic abundance has only minor effects on GagFP trafficking at low, subcooperative levels. Because per-cell Gag expression levels vary during transient transfection, we next tested the hypothesis that gRNA cytoplasmic abundance is more relevant to the assembly pathway at reduced (subcooperative) levels of Gag using HeLa cells engineered to stably express only low levels of COGag-cyan fluorescent protein (CFP) (HeLa.Gag-CFP cells). We reasoned that if HIV-1 gRNA exhibits any proassembly activity (by either nucleating assembly or having a low activation energy necessary to initiate VLP assembly), gRNAs might lower the cooperative threshold by collecting and/or compartmentalizing Gag molecules even at low whole-cell concentrations.

To test this hypothesis, we devised a system for studying gRNA abundance in HeLa cells that were engineered to stably express only low, subcooperative levels of COGag-CFP (HeLa.Gag-CFP cells). Under steady-state conditions, these cells exhibited Gag-CFP in the cytoplasm with no evidence of assembly events as defined by COGag-CFP fluorescence or diffraction-limited Gag-CFP punctae forming at the PM. However, provision of unlabeled Gag to these cells, via either HIV-1 infection (Fig. 2A, and see Movie S1 in the supplemental material) or transfection of plasmids encoding WT-MSL gRNAs (Fig. 2C), caused the COGag-CFP pool to shift markedly to the PM in cells as early as 24 to 36 h postinfection/transfection. This response was consistent with previous reports defining assembly as a cooperative process (i.e., a function of cytoplasmic Gag/Gag-Pol levels) (41, 42) and confirmed the utility of this cell line as a novel biosensor for detecting HIV-1 assembly events in real time and with single-cell resolution.

Because our HeLa.Gag-CFP cell line lacked MS2-YFP, we modified WT-MSL, 1ACG-MSL, and dRRE-MSL constructs to express MS2-mCherry-NLS from the native viral promoter (with the MS2-mCherry-NLS open reading frame inserted into the *nef* locus as indicated in Fig. 2B). In HeLa.Gag-CFP cells expressing WT-MSL/MS2-mCherry-NLS gRNAs, we observed marked transitions of COGag-CFP to discrete punctae at the PM in >75% of cells, identical to the transitions observed after infection (Fig. 2A), demonstrating recruitment of Gag-CFP into budding virions in *trans* mediated by the assembly of unlabeled Gag expressed from the WT-MSL virus (Fig. 2C, left panels, and quantification in Fig. 2D). The gRNA's MS2-mCherry-NLS signal (yellow) colocalized with surface Gag-CFP (cyan), which is consistent with Gag/gRNA cotrafficking to the PM and suggests gRNA encapsidation (Fig. 2C, bottom left panel). Gag-CFP was also released from cells as VLPs under this condition (in Fig. 2F, compare lane 2 to lane 1). Contrary to the hypothesis that gRNAs exhibit proassembly activity independently of Gag steady-state levels, accumulation of 1ACG-MSL gRNAs in the cytoplasm did not drive COGag-CFP to accumulate at the PM. Instead, we observed COGag-CFP as well as cytoplasmic MS2-mCherry-NLS signals (as a proxy marker for gRNAs) coalescing in large cytoplasmic granules in >50% of transfected cells (Fig. 2C, middle panels, and see the quantification in Fig. 2E; this is most clearly demonstrated in Movie S2). The MS2-mCherry-NLS signal was restricted to the nucleus for the dRRE-MSL condition, and as expected, this construct had no effect on COGag-CFP distribution (Fig. 2C, right panels, D, and E). Taken together, these data indicated that even if the subcooperative threshold for Gag aggregation is lowered by an excess abundance of cytoplasmic gRNA in single cells, the result is the formation of large Gag/gRNA-containing cytoplasmic granules and not stimulation of PM-targeted assembly events.

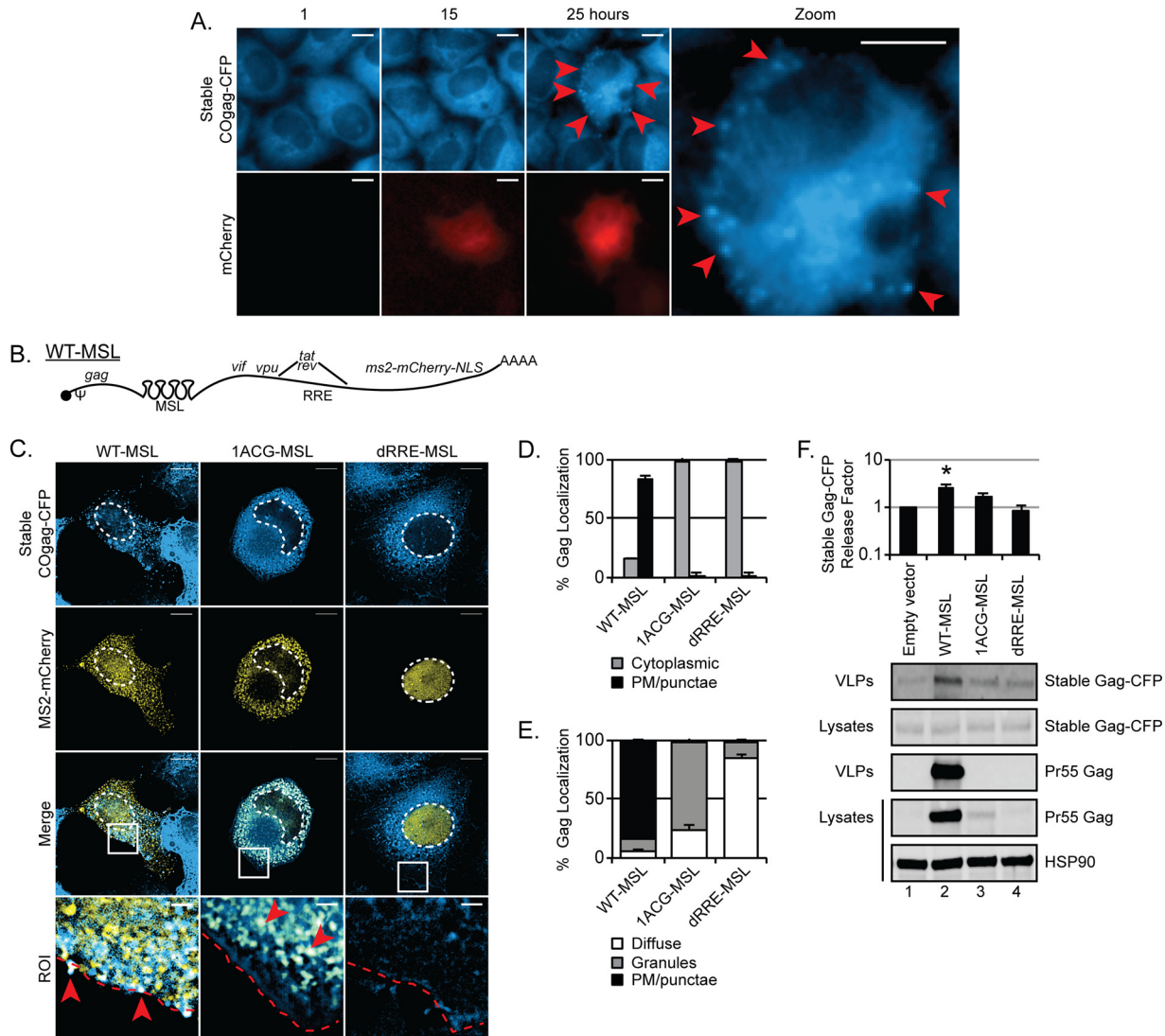


FIG 2 HIV-1 gRNA cytoplasmic abundance plays a minor role in GagFP trafficking at the subcooperative threshold. (A) Widefield deconvolution microscopy images from live-cell imaging experiments of HeLa.Gag-CFP cells infected with the WT NL4-3/E-R-mCherry reporter virus. Multichannel images were acquired once per hour for up to 48 h beginning at ~1 h postinfection. Scale bars represent 10 μ m. Red arrowheads indicate sites where stably expressed COGag-CFP has transitioned from a diffuse cytoplasmic distribution to PM-associated punctae. (B) Depiction of "self-labeling" WT-MSL gRNA. These gRNAs are identical to those depicted in Fig. 1A with the addition of MS2-mCherry-NLS as a reporter and gRNA-tagging protein expressed from the viral *nef* gene position. (C) Widefield deconvolution microscopy images of stable HeLa.Gag-CFP cells transfected with 1,000 ng HIV gRNA constructs and fixed ~30 h posttransfection. Scale bars represent 10 μ m in full images and 2 μ m in regions of interest. Dashed white lines show the relative positions of cell nuclei. The white box designates the regions of interest. Red arrowheads indicate sites where stably expressed Gag-CFP has accumulated at the PM for WT-MSL or in the cytoplasm for 1ACG-MSL. dRRE-MSL gRNAs are not exported from the nucleus. The dashed red line in regions of interest represents the edge of cell. (D and E) Quantification of Gag-CFP distribution phenotypes from live-cell imaging experiments performed as described for panel A. HeLa.Gag-CFP cells were transfected with 333 ng of gRNA constructs (WT-MSL, 1ACG-MSL, and dRRE-MSL also encoding MS2-mCherry-NLS as a reporter and gRNA tagging protein). (D) Bar graphs show the percentages of transfected cells with diffuse or PM-adjacent punctae during Gag localization. (E) Bar graph shows the percentages of transfected cells with diffuse granules or PM-adjacent punctae during Gag localization. Error bars represent standard deviations from the means. At least 30 cells were quantified per transfection condition per experiment ($n = 3$). (F) HEK293T.Gag-CFP cells were transfected with 2,000 ng of HIV gRNA constructs (as indicated) or an empty-vector control (pBluescript) and immunoblotted for Gag and HSP90. Bar graphs show fold changes in Gag release factor (\log_{10} scale) relative to levels under empty-vector conditions ($n = 3$). The asterisk indicates that expression of the stable Gag-CFP release factor for the WT-MSL condition is significantly different from that for the empty-vector condition (two-tailed Student's *t* test, $P = 0.0006$).

Perturbing the subcellular localization of HIV-1 gRNAs competent for Gag synthesis disrupts virus particle production. Having ruled out *trans*-mediated proassembly signals attributable to net gRNA abundance in the cytoplasm, we next tested whether directly perturbing the subcellular localization of gRNAs would affect Gag trafficking or sites of virion assembly. To this end, we modified MS2-YFP fusion proteins

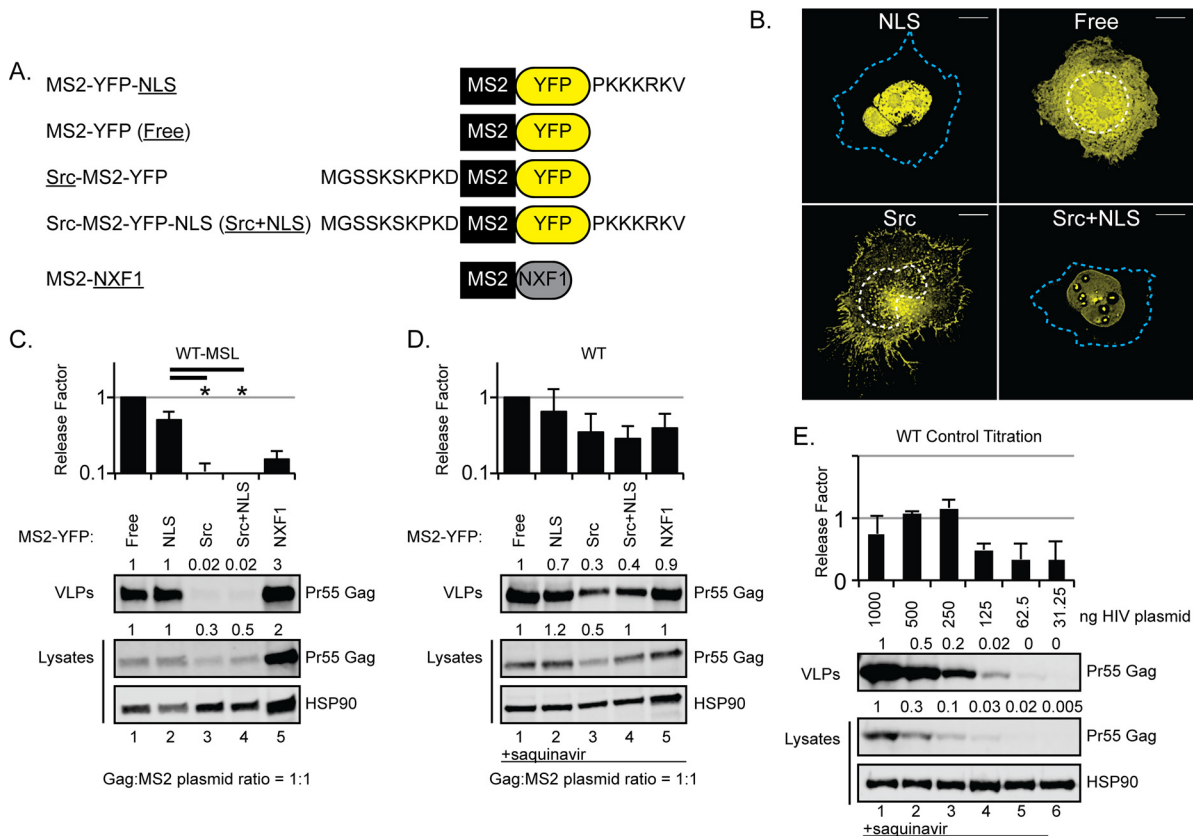


FIG 3 Perturbing HIV-1 gRNA subcellular localization disrupts virus particle production. (A) Cartoon depiction of MS2-YFP targeting protein constructs used in these studies. The short names used in subsequent images are underlined. The amino acid-targeting motifs are shown at their relative (amino- or carboxy-terminal) positions. (B) Widefield deconvolution microscopy images of HeLa cells transfected with 333 ng MS2-YFP targeting constructs and fixed ~30 h posttransfection. Scale bars represent 10 μ m. Dashed white lines show the relative positions of cell nuclei. Dashed cyan lines show the edge of the cell. (C) HEK293T cells were transfected with 1,000 ng MS2-YFP targeting constructs as indicated and 1,000 ng of WT MSL and immunoblotted for Gag and HSP90. Bar graphs show the release factors (\log_{10} scale) relative to the release of Free MS2-YFP. Error bars represent standard deviations from the means of results from three independent experiments. The asterisks indicate that the Pr55 Gag release factors are significantly different for comparisons indicated by black bars (by the two-tailed Student *t* test, $P = 0.023$ for the comparison with Src and 0.015 Src plus NLS). (D) HEK293T cells were transfected with 1,000 ng MS2-YFP targeting constructs as indicated and 1,000 ng of WT NL4-3/E-R and immunoblotted for Gag and HSP90. Cells were treated with the HIV-1 protease inhibitor saquinavir to prevent Pr55 Gag proteolytic processing and aid quantification of Gag expression and release. Bar graphs show release factors (\log_{10} scale) relative to the release of Free MS2-YFP. Error bars represent standard deviations from the means of results from three independent experiments. No conditions were significantly different. (E) HEK293T cells were transfected with the indicated amounts of the WT NL4-3/E-R plasmid and processed as described for panel D. Bar graphs show release factors (arithmetic scale) relative to release under the 1,000-ng condition. Error bars represent standard deviations from the means from three independent experiments. (C to E). Numbers above blot images represent Gag intensity values of the band directly below, relative to the intensity in lane 1 of each image.

to carry subcellular trafficking motifs in order to artificially target MSL-bearing gRNAs to specific cellular membranes or the actin cytoskeleton (Fig. 3 to 6). To target the gRNAs to cellular membranes, we first tested a protein myristylation signal (MGSSKSKPKD) derived from the proto-oncogene Src kinase, fused to MS2-YFP (Src-MS2-YFP). The Src targeting motif was chosen for these experiments because, as in Gag's MA domain, it targets proteins to PI(4,5)P₂ phospholipid moieties present at the cytoplasmic face of the PM (87). Indeed, prior work has shown that the assembly of Gag mutants lacking MA is rescued by the addition of an amino-terminal Src membrane targeting motif (41, 70). We generated versions of Src-MS2-YFP that would or would not accumulate preferentially in association with the nucleus due to the presence or absence of a carboxy-terminal NLS (Src-MS2-YFP and Src-MS2-YFP-NLS, respectively) (Fig. 3A). We also employed a previously validated MS2-NXF1 fusion protein that alters gRNA nucleocytoplasmic transport by biasing it toward the NXF1/NXT1 nuclear export pathway, in competition with Rev and CRM1 (88, 89). Fluorescence microscopy confirmed that the Src-MS2-YFP protein localized predominantly to the PM when expressed alone in cells,

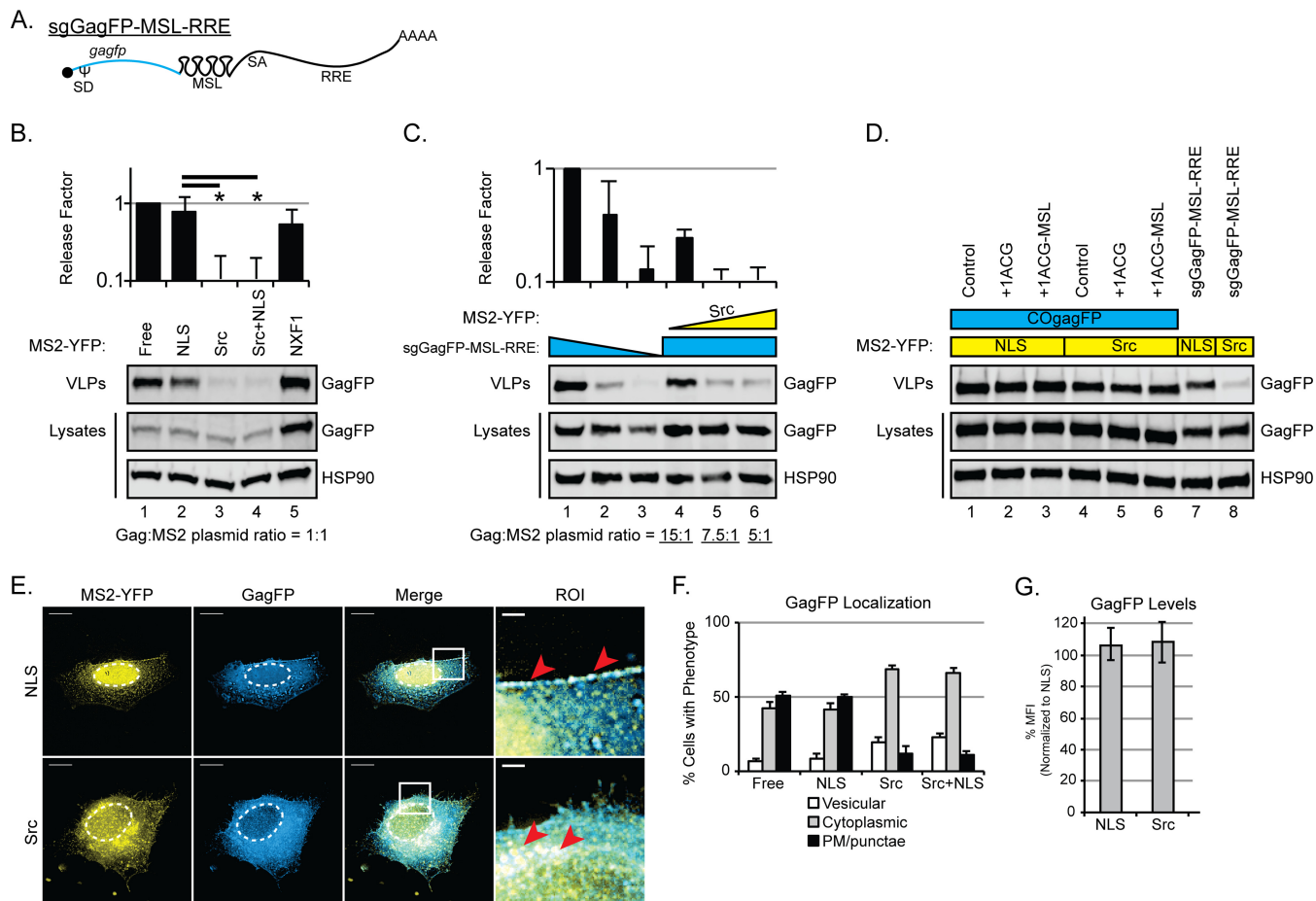


FIG 4 Src-MS2-YFP proteins induce a gRNA-specific block to Gag trafficking in *cis*. (A) Cartoon depiction of the subgenomic HIV-1 sgGagFP-MSL-RRE construct used. The splice donor (SD) and splice acceptor (SA) are shown to emphasize that the viral gagFP mRNA (surrogate subgenomic gRNA) retains an intron. (B) HEK293T cells were transfected with 1,000 ng MS2-YFP targeting constructs as indicated, 900 ng of sgGagFP-MSL-RRE, and 100 ng pRev and immunoblotted for Gag and HSP90. Bar graphs show release factors (\log_{10} scale) relative to the release of Free MS2-YFP. Error bars represent standard deviations from three independent experiments. The asterisks indicate that the Gag release factors are significantly different for comparisons indicated by black bars (by the two-tailed Student *t* test, $P = 0.03$). (C) HEK293T cells were transfected with decreasing amounts of sgGagFP-MSL-RRE (1,500/1,000/500 ng) plus 200 ng Rev and the empty vector as a filler up to 2 μ g total DNA in lanes 1 to 3. Cells were transfected with 1,500 ng sgGagFP-MSL-RRE plus 200 ng Rev, the empty vector as a filler, and increasing amounts (100/200/300 ng) of Src-MS2-YFP and immunoblotted for Gag and HSP90 in lanes 4 to 6. Bar graphs show release factors (\log_{10} scale) relative to the release in lane 1. Error bars represent standard deviations from the means of results from three independent experiments. (D) *cis* versus *trans* effects. HEK293T cells were transfected with 500 ng of COgag-CFP, 100 ng of the indicated MS2-YFP targeting construct, and 1,400 ng of the empty vector, 1ACG (no MSL), or 1ACG-MSL in lanes 1 to 6. Lanes 7 to 8 were transfected with 1,400 ng of sgGagFP-MSL-RRE, 100 ng of the indicated MS2-YFP targeting construct, 200 ng of Rev, and 300 ng of the empty vector immunoblotted for Gag and HSP90. (E) Widefield deconvolution microscopy images of HeLa cells transfected with 100 ng MS2-YFP targeting constructs, 800 ng subgenomic sgGagFP-MSL-RRE, and 100 ng pRev and fixed ~30 h posttransfection. Scale bars represent 10 μ m in full images and 2 μ m in regions of interest (ROI). Dashed white lines show the relative positions of cell nuclei. White boxes outline the regions of interest. Red arrowheads indicate sites where GagFP has accumulated. (F) Quantification of GagFP localization phenotypes. Bar graphs show the percentages of cells exhibiting vesicular, diffuse cytoplasmic, or PM-associated puncta for each transfection condition. Error bars represent the standard deviations from the means of results for three independent experiments, with quantification of at least 100 cells per condition. (G) Whole-field quantification of GagFP fluorescence for ~500 cells comparing the permissive NLS and nonpermissive Src-MS2-YFP conditions in cells fixed and imaged at 24 h posttransfection. HeLa cells were transfected with 150 ng of the MS2-YFP targeting construct, 750 ng of sgGagFP-MSL-RRE, and 100 ng of pRev. Error bars represent the standard deviations from the means from three independent transfections.

as expected (Fig. 3B). Interestingly, the addition of the NLS (Src-MS2-YFP-NLS) resulted in preferential targeting to the nuclear membrane (Fig. 3B), perhaps accessing nucleus-associated PI(4,5)P₂ (90).

We initially hypothesized that the MS2-YFP protein bearing the Src membrane targeting signal would stimulate virus particle assembly by enhancing MSL-dependent gRNA trafficking to the PM and thus provide a nucleation signal to Gag. However, we observed the opposite outcome, with coexpression of either Src-MS2-YFP or Src-MS2-YFP-NLS causing a >10-fold reduction in the VLP release of Gag derived from MSL-bearing gRNA (WT-MSL) transcripts (in Fig. 3C, compare lanes 3 and 4 to lanes 1 and 2).

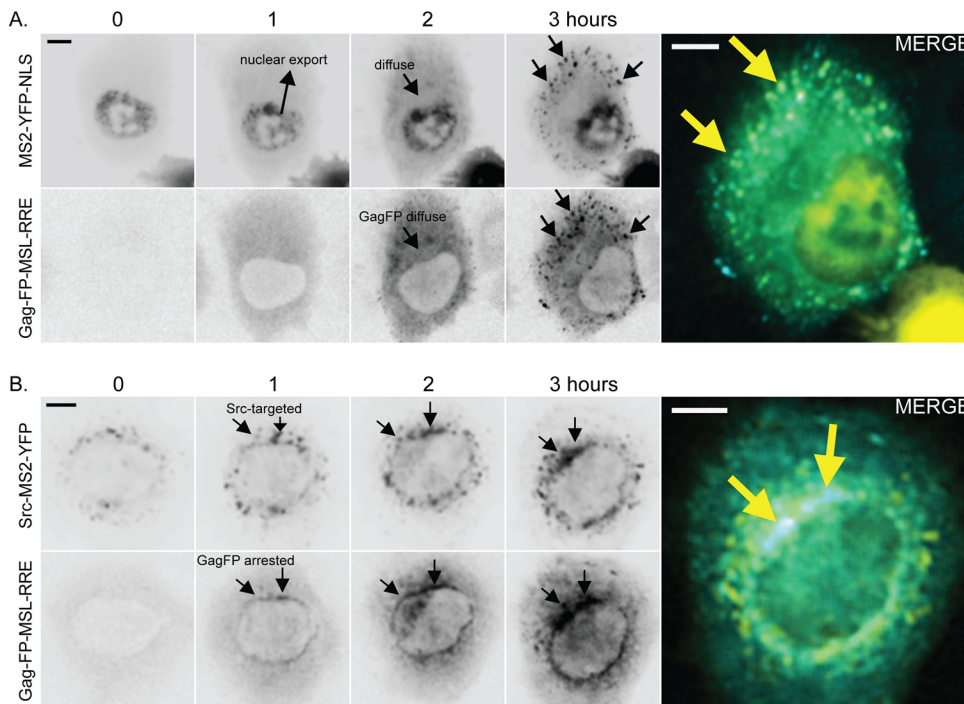


FIG 5 Mistargeted gRNAs are capable of physically rerouting Gag trafficking to aberrant subcellular locations even at very low levels of Gag expression. (A) Single HeLa cells expressing GagFP derived from sgGagFP-MSL-RRE constructs, Rev, and MS2-YFP-NLS transfected as described for Fig. 4E and monitored using live-cell fluorescence microscopy. Multichannel images were acquired once per hour for up to 16 h beginning at ~6 h posttransfection. Times indicated are hours since the first observation of GagFP expression. Both GagFP and MS2-YFP signals accumulated in the cytoplasm over time prior to coalescing in bright punctae at the PM. (B) When coexpressed with the Src-MS2-YFP protein, both Src-MS2-YFP and GagFP aggregated in a perinuclear zone at even the lowest levels of GagFP detected (see images at 0 and 1 h). Yellow arrows in panels on the right indicate colocalization (white) of Src-MS2-YFP (yellow) and GagFP (cyan) at the 3-h time point.

Parental WT gRNAs lacking the MSL cassette were relatively immune to the MS2 targeting proteins (Fig. 3D), even at a high ratio (1:1) of MS2 to gRNA plasmids, thus demonstrating that the bulk of the effect was specific to MS2-MSL interactions. Indeed, lysate levels of Gag were relatively constant among MS2-YFP targeting conditions, while total Gag levels (VLP plus lysate) from the WT-MSL gRNAs were inhibited by Src-MS2-YFP and Src-MS2-YFP-NLS. As Gag modulates its own translation such that translation is inhibited at high concentrations of Gag, one would not necessarily expect a defect in assembly and release to always result in equivalent accumulations of intracellular Gag (91). Furthermore, the MS2-NXF1 also affected VLP release specifically from the WT-MSL construct. This effect was associated with a marked increase in levels of cell-associated Gag, likely reflecting enhanced gRNA nuclear export and/or effects on gRNA trafficking or Gag steady-state levels intrinsic to the N XF1/NXT1 pathway (Fig. 3C, lane 5).

Because assembly is a cooperative process (i.e., highly sensitive to intracellular Gag levels) (12, 41, 43), we sought to further test if the effects on virus particle production reflected either (i) net reductions in Gag expression levels, (ii) decreases in Gag assembly efficiency, or (iii) a combination of both effects. In our experiments, we measured virus assembly competency by calculating a release factor (79), defined as the amount of Gag detected in VLPs released into the culture medium (determined by quantitative infrared immunoblotting), and compared its levels to levels of cell-associated Gag. Careful control titrations of the WT construct from 1,000 ng to 31.25 ng per transfection (Fig. 3E) demonstrated a remarkably linear ($R^2 = 0.97$) relationship between Gag cytoplasmic abundance and VLP production at all levels of Gag in our assays (i.e., a 10-fold loss in VLP production correlated with a 10-fold decrease in cytoplasmic Gag abundance) (in Fig. 3E, compare lane 1 to lane 3). For the Src-MS2-YFP

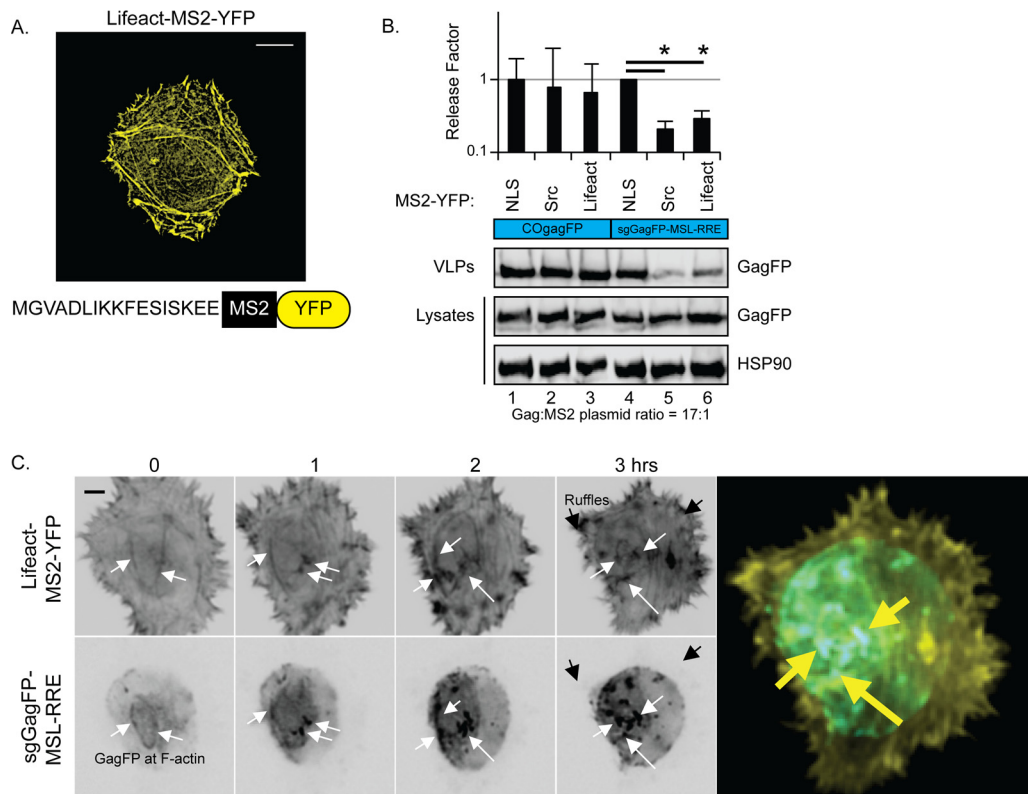


FIG 6 Effects of retargeting gRNAs to the actin cytoskeleton. (A) Cartoon depiction of the Lifeact-MS2-YFP targeting protein construct and widefield deconvolution microscopy image of a HeLa cell transfected with 333 ng MS2-YFP targeting constructs, fixed ~30 h posttransfection. The scale bar represents 10 μ m. (B) HEK293T cells were transfected with 100 ng of the indicated MS2-YFP targeting constructs and either 1,700 ng COGagFP (no MSL) with 200 ng of the empty vector or 1,700 ng of sgGagFP-MSL-RRE with 200 ng pRev and immunoblotted for Gag and HSP90. Bar graphs show release factors (\log_{10} scale) relative to the release under the MS2-YFP-NLS condition for each Gag type (COGagFP or sgGagFP-MSL-RRE). Error bars represent standard deviations from the means of results from three independent experiments. The asterisks indicate that the GagFP release factors are significantly different for comparisons indicated by black bars (by the two-tailed Student *t* test, $P = 0.0001$). (C) Images from live-cell time-lapse fluorescence microscopy of a HeLa cell expressing GagFP derived from 750 ng sgGagFP-MSL-RRE constructs cotransfected with 100 ng Rev and 150 ng Lifeact-MS2-YFP. Multichannel images were acquired once per hour for up to 16 h beginning at ~6 h posttransfection. Times indicated are hours since the first observation of GagFP expression. Gag aggregated with linear F-actin bundles at or near the cell surface even at early time points (0 h). Yellow arrows in the panel on the right indicate colocalization (white) of Lifeact-MS2-YFP (yellow) and GagFP (cyan) at the 3-h time point.

conditions, we observed an ~2-fold reduction in cell-associated Gag for both the WT-MSL and WT constructs (e.g., in Fig. 3C, compare lanes 3 and 4 to Fig. 3D, lane 3). However, the effects on VLP release for the MSL-bearing construct were much greater (>10-fold compared to 3-fold) (in Fig. 3C, compare VLPs in lanes 3 and 4 to those in Fig. 3D, lane 3). Thus, while Src-MS2-YFP interactions with WT-MSL gRNAs modestly affected Gag steady-state levels, virus particle release was dramatically inhibited. All together, these data suggested that the decreases in virus assembly presented in Fig. 3 were due largely to decreased Gag assembly and release, coupled with modest net reductions in Gag expression levels.

Tethering gRNAs to non-PMs disrupts Gag's trafficking to the plasma membrane. To address the mechanism underpinning the Src-MS2-YFP effects on Gag abundance and trafficking, we directly monitored Gag in single cells using previously validated, intron-retaining and Rev-dependent GagFP-MSL-RRE surrogate gRNA (sg) transcripts (81) (Fig. 3 to 7). As with WT-MSL gRNAs, sgGagFP-MSL-RRE VLP release was completely inhibited by Src-MS2-YFP or Src-MS2-YFP-NLS proteins (Fig. 4B, compare lanes 3 and 4 to lanes 1 and 2). Increasing the ratio of Src-MS2-YFP to gRNA plasmids lowered the amount of GagFP released from cells in the form of VLPs without changing levels of cell-associated GagFP (Fig. 4C, lanes 4 to 6), a result, again, consistent with a block of virus particle assembly or release from the cell.

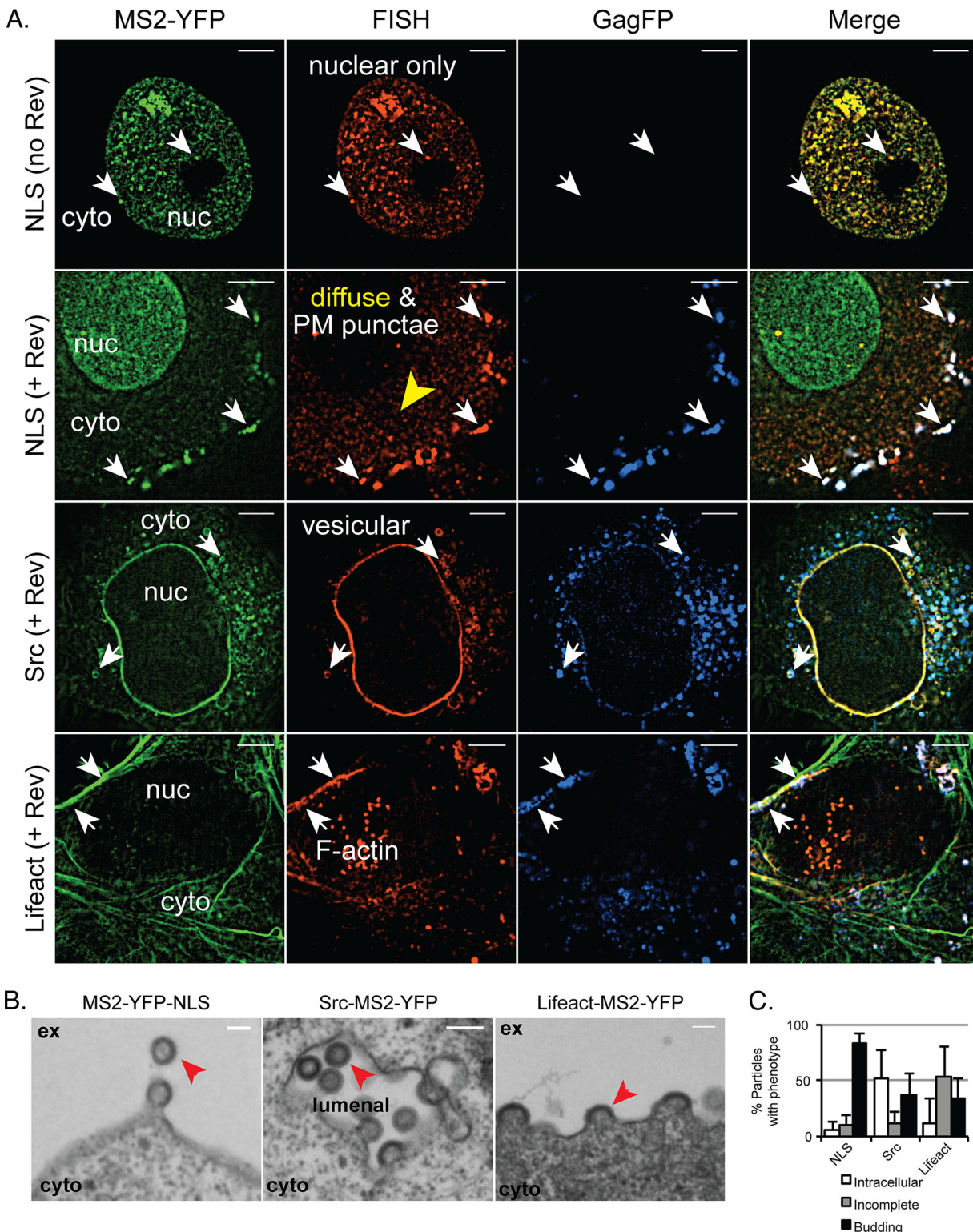


FIG 7 gRNA-directed effects on Gag trafficking and subcellular sites of virus particle assembly. (A) HeLa cells were transfected with 800 ng of sgGagFP-MSL-RRE, 100 ng of the indicated MS2-YFP targeting constructs, and 100 ng of Rev or the empty vector, as indicated. Cells were fixed at ~30 h posttransfection and subjected to FISH, and multi-Z-stack images were acquired by structured-illumination microscopy (SIM) using 100× (NA, 1.49) TIRF oil objective. Single Z-plane images are shown, with scale bars representing 5 μm. White arrows indicate points of interest highlighting colocalization. nuc, nucleus; cyto, cytoplasm. (B) HEK293T cells were transfected with 1,800 ng WT-MSL and 200 ng MS2-YFP targeting constructs as indicated for EM. Red arrowheads indicate representative particle events for budding (NLS), intracellular (Src), and incomplete (Lifeact) conditions. ex, extracellular. (C) Quantification of particles with budding phenotypes observed by thin-section EM. The bar graph shows percentages of assembly events exhibiting the intracellular, incomplete, or budding phenotype. Errors bars represent standard deviations from the means of results, with 10 cells imaged. At least 100 budding events were quantified per condition.

We then tested whether Src-MS2-YFP proteins could inhibit VLP production in *trans* by cotransfected COGagFP with 1ACG genomes either lacking or bearing the MSL cassette and also tested them in the presence or absence of either control MS2-YFP-NLS or inhibitory Src-MS2-YFP proteins. Src-MS2-YFP did not inhibit assembly by COGagFP under these conditions (in Fig. 4D, compare lanes 3 and 6 to the sg controls in lanes 7 and 8), thus indicating that Src-MS2-YFP-induced, gRNA-dependent assembly inhibition occurs preferentially in *cis*, in the context of the *gag/gag-pol* mRNA.

Fluorescence microscopy revealed GagFP to be less frequently detected at PM punctae in the presence of Src-MS2-YFP (measured at 24 h posttransfection) than in its absence, and Gag as well as Src-MS2-YFP was most often found associated with cytoplasmic vesicles (Fig. 4E, and see the quantification in Fig. 4F). This result was consistent with the capacity of the Src-derived trafficking motif to track PI(4,5)P₂ throughout the endocytic pathway (90, 92). Fluorescence-based measurements of GagFP demonstrated no differences in cell-associated Gag at this low, yet inhibitory, ratio of Src-MS2-YFP to gRNA plasmids (1:5) (Fig. 4G). Time-lapse imaging of both MS2-YFP and GagFP constructs simultaneously in single cells revealed that, for the control MS2-YFP-NLS protein, Gag filled the cytoplasm gradually prior to the formation of bright Gag- and gRNA-positive punctae at the PM. This was consistent with the expected punctuated burst of gRNA nuclear export, Gag translation, and Gag/gRNA diffusion in the cytoplasm and ultimately with the formation of high-order assembly intermediates at the PM (Fig. 5A, black arrows). In contrast, the Src-MS2-YFP protein drove GagFP to accumulate at perinuclear structures, visible even at the lowest levels and earliest times of GagFP detected (Fig. 5B, black arrows). We concluded from these experiments that a convergence of Src-MS2-YFP, gRNA, and Gag leads to the aggregation of Gag/gRNA transport complexes at non-PMs. Gag was seen to accumulate with the Src-MS2-YFP signal even at the earliest time points, and this suggested that Gag accumulates in close proximity to its mRNA and localized site of translation. Such a behavior is less likely to occur for Gag and gRNA when they are expressed in *trans* (as suggested by Fig. 2 and consistent with the results shown in Fig. 4D).

Effects of targeting *gag-pol* mRNAs to the actin cytoskeleton. The experiments described above indicated that Src-MS2-tethered *gag-pol* mRNAs (as represented by the surrogate subgenomic GagFP gRNA transcripts) physically mislocalize Gag away from typical cytoplasmic diffusion paths directed toward the PM (Fig. 5A) to alternative locations (Fig. 5B). To further test the capacity of gRNAs to control Gag trafficking, we tested a second targeting protein, Lifeact-MS2-YFP, intended to bias gRNA trafficking to the cell periphery due to its strong interactions with the cortical actin cytoskeleton (Fig. 6). Several studies have implicated cortical actin in HIV-1 trafficking/assembly (93–98). Lifeact is a 17-amino-acid peptide capable of binding to and targeting F-actin bundles with high specificity and without disrupting actin dynamics during timespans in our studies (99). As expected, Lifeact-MS2-YFP localized to peripheral actin fibers when expressed alone in cells (Fig. 6A). Both Src-MS2-YFP and Lifeact-MS2-YFP had inhibitory effects on assembly from sgGagFP-MSL-RRE but not COGagFP (Fig. 6B), although Lifeact-MS2-YFP was typically less potent than Src-MS2-YFP (in Fig. 6B, compare lanes 5 and 6 to lane 4; Fig. 8). Two-color time-lapse single-cell imaging confirmed that GagFP was rapidly targeted to actin fibers with Lifeact-MS2-YFP, again at the earliest and lowest detectable levels of GagFP expression (Fig. 6C, white arrows). Interestingly, at early time points, GagFP clustered preferentially with Lifeact-MS2-YFP at F-actin bundles at or near the cell body (the rounded portion of the cell) and was less frequently observed in association with dynamic actin ruffles or filopodia at the cell periphery (Fig. 6C, black arrows at 3 h). These experiments confirmed that retargeted *gag-pol* mRNAs are sufficient to target Gag to even relatively exotic subcellular locales, such as the actin cytoskeleton.

Targeting *gag-pol* mRNAs to non-PMs or the actin cytoskeleton alters sites of virus particle assembly. Because the MS2-YFP proteins were proxies for MSL-bearing RNAs, it was essential to confirm the subcellular localization of native gRNAs using

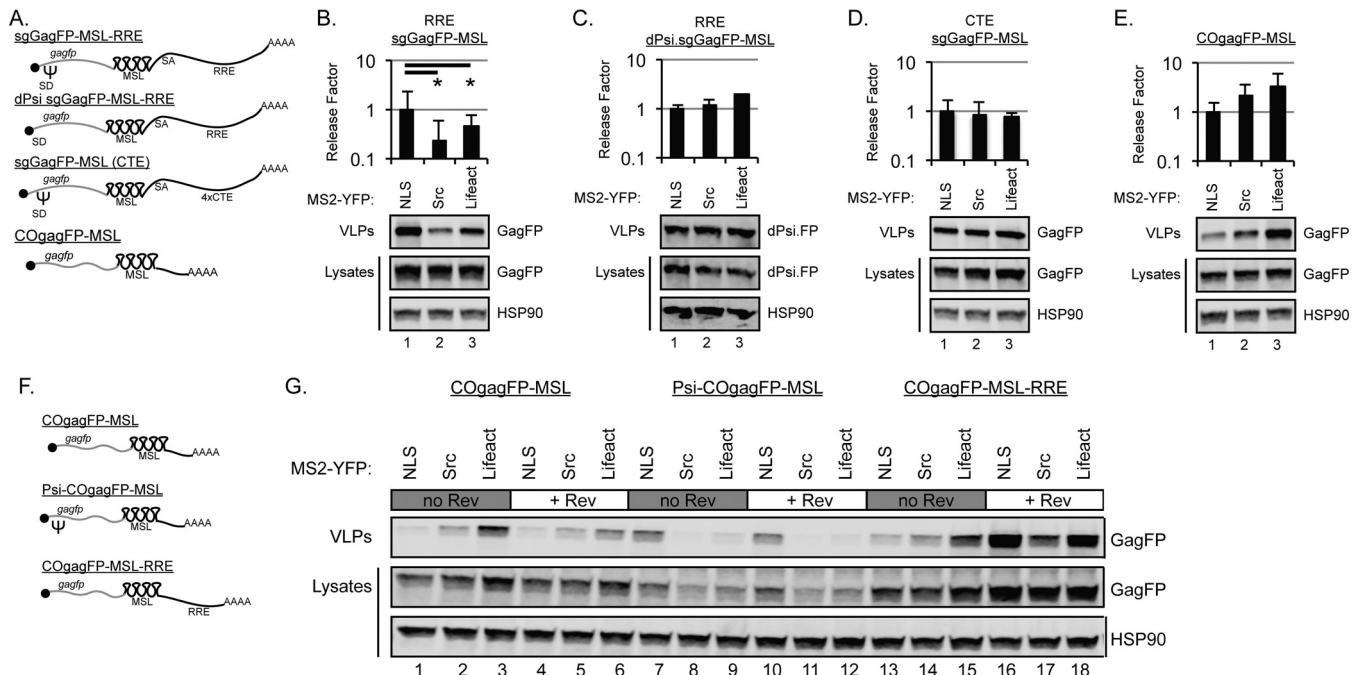


FIG 8 The HIV-1 gRNA's capacity to regulate Gag trafficking maps to both Psi and the RRE. (A) Cartoon depiction of constructs used in these studies. 4×CTE, four copies of the constitutive transport element from Mason-Pfizer monkey virus. (B to E) HEK293T cells were transfected with 100 ng of the MS2-YFP targeting constructs, as indicated, 1,700 ng of sgGagFP-MSL-RRE, and 200 ng pRev (B); 1,700 ng of dPsi.sgGagFP-MSL-RRE and 200 ng of pRev (C); 1,700 ng of sgGagFP-MSL-CTE and 200 ng of the empty vector (D); or 1,700 ng of CoGagFP-MSL and 200 ng of the empty vector (E). VLPs and cell lysates were immunoblotted for Gag and HSP90. Bar graphs show release factors (\log_{10} scale) relative to the release of MS2-YFP-NLS. Error bars represent standard deviations from the means of results from three independent experiments. The asterisks indicate that GagFP release factors are significantly different for comparisons indicated by black bars (by the two-tailed Student *t* test, $P = 0.018$ in a comparison with Src and 0.047 Lifeact). (F) Cartoon depiction of COGagFP constructs used in the experiment in panel G. (G) HEK293T cells were transfected with 100 ng of the indicated MS2-YFP targeting constructs, 1,700 ng of the indicated COGagFP constructs, and 200 ng of either the empty vector or pRev, as indicated, and immunoblotted for Gag and HSP90.

single-molecule fluorescence *in situ* hybridization (smFISH) in conjunction with super-resolution structured illumination microscopy (SIM). In these 3-color experiments, we transfected HeLa cells with Rev-dependent sgGag-FP-MSL-RRE and MS2-YFP fusion proteins either with or without Rev, fixed cells at ~30 h posttransfection, and performed smFISH using a *gag/gag-pol*-specific DNA probe set (Fig. 7A). HeLa cells transfected with MS2-YFP-NLS and sgGag-FP-MSL-RRE in the absence of Rev exhibited marked colocalization between MS2-YFP-NLS and the gRNA FISH signal in the nucleus, with no apparent GagFP expression, consistent with robust transcription but the inability of these intron-retaining mRNAs to escape the nucleus through the CRM1 export pathway (Fig. 7A, NLS without Rev condition, and see Movie S3). When Rev was coexpressed, both the MS2-YFP-NLS and gRNA FISH signals shifted to the cytoplasm, consistent with nuclear export, and were then readily detected in a diffuse distribution throughout the cytoplasm, as well as colocalizing with GagFP at PM-adjacent punctae (Fig. 7A, NLS with Rev condition, and see Movie S4). These control experiments confirmed that the MS2-YFP signals tracked in Fig. 1 to 6 were indeed representative of actual gRNA trafficking.

As expected, Src-MS2-YFP also colocalized with the gRNA smFISH signal. However, for this condition, the Src modification triggered a massive relocalization of gRNAs from a diffuse cytoplasmic distribution to perinuclear membranes, including, apparently, the nuclear envelope itself (Fig. 7A, Src with Rev condition, and see Movie S5). Consistently with the time-lapse imaging presented in Fig. 4B, we observed notable accumulations of GagFP at or near the perinuclear sites (Fig. 7A, compare blue panels for the NLS with Rev and Src with Rev conditions). Moreover, thin-section electron microscopy (EM) of HEK293T cells transfected with WT-MSL- and MS2-YFP targeting constructs confirmed a high frequency of intracellular VLP assembly events for the Src-MS2-YFP condition relative to that with the MS2-YFP-NLS control (50% of particles were detected in

association with intracellular vesicles) (Fig. 7B, and see the quantification in Fig. 7C). Thus, gRNA-directed Gag trafficking to the “wrong” cellular membranes was likely to explain the bulk of the virus particle release defect observed for Src-MS2-YFP-retargeting gRNAs. Interestingly, Lifeact-MS2-YFP clearly did not abolish Gag’s trafficking to the PM (Fig. 7A and Movie S6). However, we observed a large number of partially budding structures at the cell surface for this condition (defined as electron-dense shells less than 75% complete) (Fig. 7B and C). Thus, Gag tethered to actin filaments through its mRNA may be sufficient to confer an assembly defect. Taken together, these high-resolution imaging strategies provided further confirmation that redirecting *gag-pol* mRNAs to aberrant sites in the cytoplasm can markedly affect Gag subcellular distribution and alter the site or morphology of virus particles during assembly.

HIV-1 gRNA capacity to influence Gag trafficking maps to both Psi and the RRE.

The finding that gRNA trafficking influences the subcellular distribution of its protein product is consistent with a model wherein localized translation allows gRNAs to help compartmentalize Gag to the bud site. gRNAs encode two well-characterized *cis*-acting trafficking elements: Psi, which is encoded within the 5' UTR and bound by Gag to facilitate gRNA encapsidation (22, 33), and the RRE, which is essential for the nuclear export of gRNAs and other intron-retaining mRNAs (55, 56) (e.g., Fig. 8A). As such, we performed loss-of-function/inhibition experiments by modifying our surrogate gRNA constructs. We compared the effects of MS2 targeting proteins at relatively low MS2-to-gRNA plasmid ratios (1:17) on WT *gag-pol* mRNAs, a version mutated to no longer encode Psi (dPsi.sgGag-FP-MSL-RRE), and a version that retained Psi but was rendered Rev independent by replacement of the RRE with four copies of the constitutive transport element (CTE) derived from Mason-Pfizer monkey virus, which is well known to direct mRNA nuclear export to the NXF1/NXT1 pathway (depicted in Fig. 8A) (75, 100, 101). To our surprise, neither Src-MS2-YFP nor Lifeact-MS2-YFP had a negative effect on the assembly or release of Gag derived from the dPsi mutant transcript (compare Fig. 8B and C) and exerted only mild effects on the CTE condition (Fig. 8D). In these experiments, translation of Gag was not inhibited by Src- nor Lifeact-MS2-YFP.

Next, we performed gain-of-inhibition experiments by using COGagFP as a nonviral base *gag-pol* mRNA. We tested a dual Psi- and RRE-minus condition, using a transcript encoding codon-optimized COGagFP (as for Fig. 1A) but augmented to carry the 24-copy MSL cassette in the 3' UTR (COGagFP-MSL) (depicted in Fig. 8A). Interestingly, both Src-MS2-YFP and Lifeact-MS2-YFP actually enhanced VLP production for Gag derived from this construct (Fig. 8E and G, lanes 1 to 6). Genetic manipulation of this COGagFP-MSL construct allowed us to test the sufficiency of either RNA element (Psi and/or RRE) to affect Gag trafficking. Gag derived from COGagFP-MSL constructs modified to bear the 5' UTR region encompassing Psi (Psi plus COGagFP-MSL) (shown in Fig. 8F) became highly sensitive to Src-MS2-YFP and LifeAct-MS2-YFP expression both in terms of the cytoplasmic abundance of Gag and net VLP production (in Fig. 8G, compare lanes 7 to 9 to lanes 10 to 12). Remarkably, Gag derived from a construct modified to bear the RRE (COGagFP-MSL-RRE) (shown in Fig. 8F) also became sensitive to the Src-MS2-YFP targeting protein but only when it was expressed in the presence of Rev (in Fig. 8G, compare lanes 13 to 15 to lanes 16 to 18). Therefore, either Psi or the RRE (in the presence of Rev) structures were sufficient for Gag synthesis and/or assembly to be affected by targeting mRNAs to non-PM locations.

DISCUSSION

For retroviruses, gRNA nucleocytoplasmic transport is a tightly regulated process ensuring robust late gene expression and efficient genome encapsidation during virion assembly. Herein we provide, to our knowledge, the first direct evidence that gRNA subcellular distribution represents a core determinant of the HIV-1 virion assembly pathway. We initially hypothesized that increasing the net abundance of PM-proximal gRNAs would stimulate virus particle assembly, according to the assumption that gRNAs encode one or more signals relevant to the nucleation of assembly events at the PM (13, 32, 40). However, increasing levels of Gag-minus 1ACG-gRNAs in *trans* had

little-to-no effect on assembly either at high (Fig. 1) or low (Fig. 2) levels of COGagFP. In fact, 1ACG-gRNAs arrested COGagFP in cytoplasmic granules in our stable low-GagFP cell line, suggesting that a suboptimal Gag-gRNA stoichiometry is detrimental to the transit of gRNP-trafficking complexes.

Efforts to bias gRNP trafficking to the PM using our MS2-based RNA tethering strategy were also not beneficial to assembly but instead inhibited virus particle production for Gag derived from gRNAs as well as *Psi*- or Rev/RRE-bearing *gag-pol* mRNAs (Fig. 3 to 8). Time-resolved imaging confirmed striking changes to Gag subcellular distribution in living cells (Fig. 5B and 6C), and single-molecule fluorescence *in situ* hybridization (smFISH) coupled to superresolution microscopy in fixed cells clearly demonstrated that both the Src-MS2-YFP and the Lifeact-MS2-YFP protein markedly altered the distribution of MSL-gRNAs and Gag away from their native, "diffuse" cytoplasmic pattern to accumulate preferentially at subcellular membranes and in association with F-actin, respectively (Fig. 7A and Movies S5 and S6).

Although purposely artificial, the MS2-tethering strategy provides for comparative measurements of mRNA trafficking, translation, and Gag function in single cells, thus providing useful insights relevant to the native assembly pathway. The finding that mRNA-linked effects on Gag trafficking and assembly were observed only for gRNAs or *gag-pol* mRNAs competent for Gag synthesis (Fig. 4D) bearing either *Psi* or the RRE *cis*-acting structural elements (Fig. 8) supports a *cis*-biased model of assembly wherein coordination of gRNA nuclear export, gRNA stability in the cytoplasm, localizing translation, and compartmentalized Gag-gRNA interactions regulate Gag's assembly efficiency at or near the PM. Consistently with a model that includes localized translation of Gag near assembly sites, work is under way to directly assess whether mislocalized gRNAs are truly active sites of Gag translation and, if so, for how long. Further studies are also under way to define the contributions of *cis*- and *trans*-expressed Gag during gRNA trafficking, dimerization, packaging, and particle assembly.

Altogether, many of the determinants of HIV-1 virion assembly and gRNA packaging are known (NC, *Psi*, dimerization, etc.), but the mechanism ensuring the encapsidation of a single gRNA dimer into nearly every virion is not yet understood. Furthermore, what restricts Gag from initiating assembly of gRNA-devoid particles in cells expressing gRNA is also unknown. Compartmentalization of Gag synthesis and gRNA binding in space and time may explain why gRNA encapsidation is so highly efficient despite Gag's ready capacity to bind to nonviral RNAs and assemble noninfectious particles in the absence of gRNA binding. At early time points, we speculate that Gag and gRNAs are maintained in the cytoplasm at low abundance in order to avoid nucleating the formation of cytoplasmic granules that may represent kinetically trapped (dead-end) complexes (Fig. 2D and Movie 3). Low-order Gag-gRNA interactions may control how much Gag is translated (91), and diffusion in the cytoplasmic fluid will ultimately allow assembly intermediates to achieve close proximity to the PM (102–104). The finding that mistargeted gRNAs are capable of "dragging" Gag to (and/or translate Gag at) aberrant locales and, in some instances, perturbing the efficiency of budding (note the partial capsids for the Lifeact condition shown in Fig. 7B) suggests a strong physical interaction. In this context, *Psi*'s role while bound by Gag likely explains why this element is both necessary and sufficient to allow for MS2-mediated perturbation of Gag distribution (Fig. 8). We suggest that the presence of *Psi* increases the specificity of Gag binding to gRNAs and *gag* mRNAs and that this prevents this Gag from trafficking to other subcellular locales. That the RRE (with Rev) has a similar but less potent effect (Fig. 8G) is more intriguing. However, Gag was recently shown by Kutluay and colleagues to bind the RRE with specificity (51), and Rev and/or the RRE have previously been shown to play roles in gRNA encapsidation (53, 54, 105, 106). As such, Gag-RRE interactions may prevent Gag from trafficking away from relocalized gRNAs and *gag* mRNAs, as with *Psi*.

We emphasize that under native conditions, it is almost certain that Gag plays the dominant role in defining the preferred site of assembly by tethering gRNAs to the PM through the activity of its N-terminal matrix domain (13, 40). However, we point out

that our data do not rule out potential contributions from one or more cellular RNA binding proteins in addition to Gag that, like the MS2 targeting proteins, may modulate transient Gag/gRNA interactions with membranes or other cellular machineries. The coating and coding of mRNAs with cellular factors are well known to influence their size, hydrophobicity, fluid phase, localization, and utilization (107, 108). As such, we suggest that gRNA binding cellular proteins may regulate the movement and composition of gRNAs in concert with Gag en route to sites of and during assembly. There are already many candidate RNA binding proteins (e.g., ABCE1, DDX3, heterogeneous nuclear ribonucleoprotein [hnRNP] isoforms, RHA, Staufen, and SR proteins, among others) that have been implicated previously in the formation and maintenance of HIV-1 Gag/gRNA trafficking granules (75, 76, 79, 109–119). We also note that unique spatiotemporal features of the Rev-regulated nuclear export pathway (e.g., punctuated, rapid increases to free Gag/gRNP abundance in the cytoplasm or diffusion in itself [Fig. 5 and 6]) should influence the efficiency of the assembly pathway (81). In this context, deficiencies to one or more cofactors tied to Rev-dependent trafficking dynamics or downstream cytoplasmic events may underpin previously observed changes to Gag assembly competency when its message is rendered Rev/RRE independent (75–77, 79, 80).

In general, large gRNP complexes trafficking through the cytoplasm prior to utilization draw parallels with cellular mRNA molecules that are translated locally (2, 120, 121). Perturbations to the ability of gRNAs to freely diffuse through a dense cytoplasmic fluid may have negative consequences for localized translation and subsequent virion assembly. To date, there are no FDA-approved antiviral approaches that perturb HIV-1 gene expression or the stages upstream of immature virus particle assembly, although several strategies have been pursued, including disruption of Tat or Rev function, virus-specific miRNAs, and transdominant proteins (reviewed in reference 122). Indeed, the regulation RNP complex formation is of increasing interest in other diseases, where malformation of aberrant RNA/protein aggregates or disruption of normal fluid-phase dynamics is evident (4, 107, 123–125). Our results suggest that strategies to successfully disrupt viral mRNA subcellular distribution, gRNP complex formation, or fluid-phase transitions using small-molecule inhibitors or alternative strategies (e.g., provision of *trans*-acting synthetic “restriction” factors via gene therapy) merit further exploration.

MATERIALS AND METHODS

Cell culture, plasmids, and stable cell lines. Human HeLa and HEK293T cell lines (obtained from the ATCC) were cultured in Dulbecco's modified Eagle's medium (DMEM; Sigma-Aldrich, Madison, WI, USA) supplemented with 10% fetal bovine serum, 1% L-glutamine, and 1% penicillin-streptomycin. Full-length parental WT HIV-1 proviral plasmids were derived from the pNL4-3 molecular clone (126) bearing inactivating mutations in *env* and *vpr* and expressing a firefly luciferase reporter from the *nef* reading frame (E-R-/Luc) (127). Twenty-four copies of the MS2 bacteriophage RNA stem-loop (MSL, a kind gift of Robert Singer, Albert Einstein University, New York, NY) were engineered into the full-length pNL4-3-derived constructs as previously described (128), thereby generating pNL4-3/E-R-Luc-24×MSL (WT-MSL). Replacing the firefly luciferase reporter E-R-/Luc with mCherry in the *nef* reading frame using NotI- and Xhol-cut sites generated HIV-1/mCherry virus. sgGagFP-MSL HIV-1 expression plasmids encoded Gag fused to mTagBFP2 (129), enhanced CFP (ECFP), or mCherry upstream of the MSL cassette and inserted into surrogate, subgenomic HIV-1 gRNA plasmid Gag-Pol-Vif-RRE or Gag-Pol-Vif-4×CTE (81, 115). Rev-independent, codon-optimized Gag-fluorescent protein (COGagFP) plasmids were derived from a plasmid encoding sufficiently codon-optimized Gag-GFP (a gift of Marilyn Resh, Memorial Sloan Kettering Cancer Center, New York, NY, USA) (82, 83). The FP reading frame was fused in frame to RevInd Gag cDNAs using overlapping PCR and inserted into pcDNA3.1 using NheI- and Xhol-cut sites. In all instances, mutants of full-length HIV-1 and RevInd Gag plasmids were generated using overlapping PCR. pRevInd-GagFP-MSL was generated by inserting the 24-copy MSL cassette into pRevInd-GagFP using BsrGI-cut sites, Psi-RevInd-MSL GagFP was generated by inserting HIV-1_{NL4-3} 5' UTR nucleotides 1 to 336 into NheI and SacII sites in pCOGagFP-MSL, and pCOGagFP-MSL-RRE was generated by transferring the COGagFP-MSL sequence into a pcDNA-RRE backbone plasmid using SacI and EcoRI sites. mTagBFP2 was a gift from Michael Davidson (Addgene plasmid 55302). pRev was described previously (75). MS2-YFP targeting constructs were generated by amplifying cDNAs from pMS2-YFP (also a gift of Rob Singer, Albert Einstein University, New York, NY, USA) (130) using overlapping PCR prior to being subcloned into a pcDNA3.1 backbone using HindIII- and Xhol-cut sites. MS2-mCherry-NLS was generated by overlapping PCR to replace YFP with the mCherry reading frame and subcloned into the *nef* position of the full-length pNL4-3/E-R-Luc-24×MSL HIV constructs using NotI- and Xhol-cut sites. MS2-YFP targeting constructs included an amino-terminal membrane targeting signal derived from the Src kinase (MGSSKSKPKD) (87),

an amino-terminal Lifeact actin targeting domain (MGVADLIKKFESISKEE) (99), and/or a carboxy-terminal nuclear localization signal (NLS; PKKKRKV) derived from the SV40 Large T antigen (131). HeLa.MS2-YFP, HeLa.Gag-CFP, and HEK293T.Gag-CFP stable cell lines were generated as previously described (81, 132–134). Briefly, MS2-YFP or COGag-CFP reading frames were subcloned into a MIGR1-derived retroviral vector (pCMS28) upstream of a sequence encoding an internal ribosomal entry site (IRES) regulating a second reading frame encoding puromycin-*N*-acetyltransferase (132). High-performance clones were selected by limiting dilution in 2 µg/ml puromycin.

Retroviral assembly assays. Cells at 30 to 40% confluence were transfected with 2 µg DNA in six-well dishes using polyethylenimine (PEI; catalog no. 23966; Polysciences Inc., Warrington, PA, USA). pcDNA3.1 or pBlueScript were used as empty vector controls. Culture media were replaced at 24 h posttransfection, and cell lysates and supernatants were harvested for immunoblot analysis at 48 h as previously described (79). Briefly, 1 ml of harvested culture supernatant was filtered, underlaid with 20% (wt/vol) sucrose in PBS, and subjected to centrifugation at >21,000 × *g* for 2 h at 4°C, and viral pellets were resuspended in 35 µl dissociation buffer (62.5 mM Tris-HCl, pH 6.8, 10% glycerol, 2% sodium dodecyl sulfate [SDS], 5% β-mercaptoethanol). Cells were harvested in 500 µl radioimmunoprecipitation assay (RIPA) buffer (10 mM Tris-HCl, pH 7.5, 150 mM NaCl, 1 mM EDTA, 0.1% SDS, 1% Triton X-100, 1% sodium deoxycholate), lysed by passage through a 26-gauge needle, and subjected to centrifugation at 1,500 × *g* for 20 min at 4°C, and the liquid supernatant fraction was combined 1:1 with 2× dissociation buffer. Proteins were resolved by SDS-polyacrylamide gel electrophoresis (PAGE) and transferred to nitrocellulose membranes. Gag was detected using a mouse monoclonal antibody recognizing HIV-1 capsid/p24 (183-H12-5C; 1:1,000 dilution) from Bruce Chesebro and obtained from the NIH AIDS Research and Reference Reagent Program (Bethesda, MD, USA) (135) and anti-mouse secondary antibodies conjugated to an infrared fluorophore (IRDye680LT, 1:10,000 dilution; Li-Cor Biosciences, Lincoln, NE, USA) for quantitative immunoblotting. As a loading control, heat shock protein 90A/B (HSP90) was detected using a rabbit polyclonal antibody (H-114, 1:2,500 dilution; Santa Cruz Biotechnology, Santa Cruz, CA, USA) and anti-rabbit secondary antibodies conjugated to an infrared fluorophore (IRDye800CW, 1:7,500 dilution; Li-Cor Biosciences). Where indicated, the protease inhibitor saquinavir (NIH AIDS Research and Reference Reagent Program, Bethesda, MD) was added at 24 h posttransfection. Typically, retroviral assembly assays were performed with transfections and harvesting occurring in 1 week and with processing and immunoblotting occurring in the following week. To ensure reproducibility, most results were obtained from three biological replicates and are defined as cells plated in six-well dishes transfected on separate days (i.e., replicate 1 was transfected on a separate day from replicate 2).

Microscopy and FISH. Cells were plated in 24-well glass-bottom dishes (Mattek Corporation, Ashland, MA, USA) or 8-well microslides (IBIDI, Madison, WI, USA) and transfected using PEI. Transfection mixes contained 1 µg (24-well) or 333 ng (IBIDI) plasmid DNA, respectively. Deconvolution fixed-cell imaging experiments were performed on a Nikon Ti-Eclipse inverted wide-field microscope (Nikon Corporation, Melville, NY, USA) using a 100× Plan Apo oil objective lens (numerical aperture [NA], 1.45). These cells were fixed 24 to 32 h posttransfection in 4% paraformaldehyde in PBS. Live-cell imaging experiments were also performed on a Nikon Ti-Eclipse inverted wide-field microscope using a 20× Plan Apo objective lens (NA, 0.75) with images acquired typically every 60 min over a time course of 16 to 36 h. Images were acquired using an ORCA-Flash4.0 CMOS camera (Hamamatsu Photonics, Skokie, IL, USA) and the following excitation/emission filter sets (nanometer ranges): 430/470 (CFP), 510/535 (YFP), and 585/610 (mCherry).

For fixed-cell experiments using smFISH to visualize HIV-1 gRNA, cells were plated and transfected as described above. At ~30 h posttransfection, cells were washed, fixed in 4% formaldehyde, and permeabilized in 70% ethanol for at least 4 h at 4°C. Custom Stellaris FISH probes were designed to recognize NL4-3 HIV-1 *gag-pol* reading frame nucleotides 386 to 4614 by utilizing Stellaris RNA FISH Probe Designer (Biosearch Technologies, Inc., Petaluma, CA, USA), available online (version 4.1). The samples were hybridized with the Gag/Gag-Pol Stellaris RNA FISH probe set (48 probes) and labeled with CAL Fluor Red 610 dye (Biosearch Technologies, Inc.) according to the manufacturer's instructions available online. Structured illumination microscopy (SIM) was performed on a Nikon N-SIM microscope using a 100× total internal reflection fluorescence (TIRF) oil objective lens (NA, 1.49). Images were acquired using an Andor iXon Ultra 897 EMCCD (Andor Technology, Belfast, United Kingdom) and Nikon NIS Elements in 3D-SIM mode using the following excitation laser wavelengths (nanometer ranges): 408 (mTagBFP2), 488 (YFP), and 561 (CAL Fluor Red 610). Widefield epifluorescence microscopy images were deconvolved using NIS Elements. All images were processed and analyzed using FIJI/ImageJ2 (136). Results were obtained from three biological replicates, defined as cells plated in IBIDI slides or 24-well dishes transfected on separate days (i.e., replicate 1 was transfected on a separate day from replicate 2).

Thin-section electron microscopy. For thin-section EM, HEK293T cells were cultured in six-well dishes, transfected as described above, and processed as previously described (137). At 48 h posttransfection, cells were fixed in a solution of 2.5% glutaraldehyde, 2.0% paraformaldehyde in 0.1 M sodium phosphate buffer (PBS), pH 7.4, for ~2 h at room temperature. Samples were rinsed five times for 5 min each time in 0.1 M PBS. Rinsed cells were postfixed in 1% osmium tetroxide, 1% potassium ferrocyanide in PBS for 1 h at room temperature. Following osmium tetroxide postfixation, the samples were rinsed in PBS, as before, rinsed three times in distilled water for 5 min to clear phosphates, and embedded using increasing concentrations (10 ml A/M, 10 ml B, 300 µl C, 100 µl D components) of Durcupan ACM resin (Fluka AG, Switzerland) at 60°C. Cells were pelleted and sectioned using a Leica EM UC6 ultramicrotome, with 100-nm sections collected on 300 mesh copper thin-bar grids, and contrasted with Reynolds lead citrate and 8% uranyl acetate in 50% ethanol. Sections were observed with a Phillips CM120 transmission

electron microscope, and images were collected with a MegaView III (Olympus-SIS, Lakewood, CO, USA) side-mounted digital camera. All images were processed and analyzed using FIJI/ImageJ2 (136).

SUPPLEMENTAL MATERIAL

Supplemental material for this article may be found at <https://doi.org/10.1128/JVI.02315-16>.

TEXT S1, PDF file, 0.05 MB.

VIDEO S1, AVI file, 0.15 MB.

VIDEO S2, AVI file, 0.20 MB.

VIDEO S3, AVI file, 0.76 MB.

VIDEO S4, AVI file, 1.56 MB.

VIDEO S5, AVI file, 1.51 MB.

VIDEO S6, AVI file, 1.49 MB.

ACKNOWLEDGMENTS

This study was supported by NIH grant RO1AI110221 and a Shaw Scientist Award from the Greater Milwaukee Foundation to N.M.S. J.T.B. received support from a National Science Foundation Graduate Research Fellow program (grant DGE-1256259) and a Research Competition Award from the UW—Madison Office of the Vice Chancellor of Research and Graduate Education.

Any opinions, findings, and conclusions or recommendations expressed in this material are those of the authors and do not necessarily reflect the views of the National Science Foundation.

We gratefully acknowledge Randall Massey and the University of Wisconsin SMPH Electron Microscopy Facility for assistance with processing and imaging EM. We gratefully acknowledge Elle Kielar Grevstad and the University of Wisconsin Biochemistry Optical Core for assistance with structured illumination microscopy. The following reagents were obtained through the NIH AIDS Reagent Program, Division of AIDS, NIAID, NIH: HIV-1 p24 hybridoma (183-H12-5C) (from Bruce Chesebro) and saquinavir. We thank Bill Sugden, Sam Butcher, Ya-Fang Chiu, Halena VanDeusen, Edward Evans III, and Bayleigh Benner for their assistance in reading the manuscript and helpful intellectual discussions.

REFERENCES

- Giorgi C, Moore MJ. 2007. The nuclear nurture and cytoplasmic nature of localized mRNPs. *Semin Cell Dev Biol* 18:186–193. <https://doi.org/10.1016/j.semcd.2007.01.002>.
- Donnelly CJ, Fainzilber M, Twiss JL. 2010. Subcellular communication through RNA transport and localized protein synthesis. *Traffic* 11: 1498–1505. <https://doi.org/10.1111/j.1600-0854.2010.01118.x>.
- Buxbaum AR, Haimovich G, Singer RH. 2015. In the right place at the right time: visualizing and understanding mRNA localization. *Nat Rev Mol Cell Biol* 16:95–109. <https://doi.org/10.1038/nrm3918>.
- Beckham CJ, Parker R. 2008. P bodies, stress granules, and viral life cycles. *Cell Host Microbe* 3:206–212. <https://doi.org/10.1016/j.chom.2008.03.004>.
- Miller S, Krijnse-Locker J. 2008. Modification of intracellular membrane structures for virus replication. *Nat Rev Microbiol* 6:363–374. <https://doi.org/10.1038/nrmicro1890>.
- den Boon JA, Ahlquist P. 2010. Organelle-like membrane compartmentalization of positive-strand RNA virus replication factories. *Annu Rev Microbiol* 64:241–256. <https://doi.org/10.1146/annurev.micro.112408.134012>.
- Sundquist WI, Kräusslich HG. 2012. HIV-1 assembly, budding, and maturation. *Cold Spring Harb Perspect Med* 2:a006924. <https://doi.org/10.1101/cshperspect.a006924>.
- Freed EO. 2015. HIV-1 assembly, release and maturation. *Nat Rev Microbiol* 13:484–496. <https://doi.org/10.1038/nrmicro3490>.
- Spearman P, Wang JJ, Vander Heyden N, Ratner L. 1994. Identification of human immunodeficiency virus type 1 Gag protein domains essential to membrane binding and particle assembly. *J Virol* 68: 3232–3242.
- Zhou W, Parent LJ, Wills JW, Resh MD. 1994. Identification of a membrane-binding domain within the amino-terminal region of human immunodeficiency virus type 1 Gag protein which interacts with acidic phospholipids. *J Virol* 68:2556–2569.
- Campbell S, Rein A. 1999. In vitro assembly properties of human immunodeficiency virus type 1 Gag protein lacking the p6 domain. *J Virol* 73:2270–2279.
- Tang C, Loeliger E, Luncsford P, Kinde I, Beckett D, Summers MF. 2004. Entropic switch regulates myristate exposure in the HIV-1 matrix protein. *Proc Natl Acad Sci U S A* 101:517–522. <https://doi.org/10.1073/pnas.0305665101>.
- Jouvenet N, Simon SM, Bieniasz PD. 2009. Imaging the interaction of HIV-1 genomes and Gag during assembly of individual viral particles. *Proc Natl Acad Sci U S A* 106:19114–19119. <https://doi.org/10.1073/pnas.0907364106>.
- Ono A, Ablan SD, Lockett SJ, Nagashima K, Freed EO. 2004. Phosphatidylinositol (4,5) bisphosphate regulates HIV-1 Gag targeting to the plasma membrane. *Proc Natl Acad Sci U S A* 101:14889–14894. <https://doi.org/10.1073/pnas.0405596101>.
- Saad JS, Miller J, Tai J, Kim A, Ghanam RH, Summers MF. 2006. Structural basis for targeting HIV-1 Gag proteins to the plasma membrane for virus assembly. *Proc Natl Acad Sci U S A* 103:11364–11369. <https://doi.org/10.1073/pnas.0602818103>.
- Ono A. 2009. HIV-1 assembly at the plasma membrane: Gag trafficking and localization. *Future Virol* 4:241–257. <https://doi.org/10.2217/fvl.09.4>.
- Fuller SD, Wilk T, Gowen BE, Kräusslich HG, Vogt VM. 1997. Cryo-electron microscopy reveals ordered domains in the immature HIV-1

- particle. *Curr Biol* 7:729–738. [https://doi.org/10.1016/S0960-9822\(06\)00331-9](https://doi.org/10.1016/S0960-9822(06)00331-9).
18. Wright ER, Schooler JB, Ding HJ, Kieffer C, Fillmore C, Sundquist WI, Jensen GJ. 2007. Electron cryotomography of immature HIV-1 virions reveals the structure of the CA and SP1 Gag shells. *EMBO J* 26: 2218–2226. <https://doi.org/10.1038/sj.emboj.7601664>.
 19. Briggs JA, Riches JD, Glass B, Bartonova V, Zanetti G, Kräusslich HG. 2009. Structure and assembly of immature HIV. *Proc Natl Acad Sci U S A* 106:11090–11095. <https://doi.org/10.1073/pnas.0903535106>.
 20. Berkowitz RD, Ohagen A, Höglund S, Goff SP. 1995. Retroviral nucleocapsid domains mediate the specific recognition of genomic viral RNAs by chimeric Gag polyproteins during RNA packaging in vivo. *J Virol* 69:6445–6456.
 21. Zhang Y, Barklis E. 1995. Nucleocapsid protein effects on the specificity of retrovirus RNA encapsidation. *J Virol* 69:5716–5722.
 22. D’Souza V, Summers MF. 2005. How retroviruses select their genomes. *Nat Rev Microbiol* 3:643–655. <https://doi.org/10.1038/nrmicro1210>.
 23. Rulli SJ, Hibbert CS, Mirro J, Pederson T, Biswal S, Rein A. 2007. Selective and nonselective packaging of cellular RNAs in retrovirus particles. *J Virol* 81:6623–6631. <https://doi.org/10.1128/JVI.02833-06>.
 24. Eckwahl MJ, Arnion H, Kharytonchyk S, Zang T, Bieniasz PD, Telesnitsky A, Wolin SL. 2016. Analysis of the human immunodeficiency virus-1 RNA packageome. *RNA* 22:1228–1238. <https://doi.org/10.1261/rna.057299.116>.
 25. VerPlank L, Bouamr F, LaGrassa TJ, Agresta B, Kikonyogo A, Leis J, Carter CA. 2001. Tsg101, a homologue of ubiquitin-conjugating (E2) enzymes, binds the L domain in HIV type 1 Pr55(Gag). *Proc Natl Acad Sci U S A* 98:7724–7729. <https://doi.org/10.1073/pnas.131059198>.
 26. Garrus JE, von Schwedler UK, Pornillos OW, Morham SG, Zavitz KH, Wang HE, Wettstein DA, Stray KM, Côté M, Rich RL, Myszka DG, Sundquist WI. 2001. Tsg101 and the vacuolar protein sorting pathway are essential for HIV-1 budding. *Cell* 107:55–65. [https://doi.org/10.1016/S0092-8674\(01\)00506-2](https://doi.org/10.1016/S0092-8674(01)00506-2).
 27. Demirov DG, Ono A, Orenstein JM, Freed EO. 2002. Overexpression of the N-terminal domain of TSG101 inhibits HIV-1 budding by blocking late domain function. *Proc Natl Acad Sci U S A* 99:955–960. <https://doi.org/10.1073/pnas.032511899>.
 28. Martin-Serrano J, Zang T, Bieniasz PD. 2001. HIV-1 and Ebola virus encode small peptide motifs that recruit Tsg101 to sites of particle assembly to facilitate egress. *Nat Med* 7:1313–1319. <https://doi.org/10.1038/nm1201-1313>.
 29. Dorman N, Lever A. 2000. Comparison of viral genomic RNA sorting mechanisms in human immunodeficiency virus type 1 (HIV-1), HIV-2, and Moloney murine leukemia virus. *J Virol* 74:11413–11417. <https://doi.org/10.1128/JVI.74.23.11413-11417.2000>.
 30. Butsch M, Boris-Lawrie K. 2002. Destiny of unspliced retroviral RNA: ribosome and/or virion? *J Virol* 76:3089–3094. <https://doi.org/10.1128/JVI.76.7.3089-3094.2002>.
 31. Johnson SF, Telesnitsky A. 2010. Retroviral RNA dimerization and packaging: the what, how, when, where, and why. *PLoS Pathog* 6:e1001007. <https://doi.org/10.1371/journal.ppat.1001007>.
 32. Jouvenet N, Lainé S, Pessel-Vivares L, Mougel M. 2011. Cell biology of retroviral RNA packaging. *RNA Biol* 8:572–580. <https://doi.org/10.4161/rna.8.4.16030>.
 33. Kuzembayeva M, Dilley K, Sardo L, Hu W-S. 2014. Life of psi: how full-length HIV-1 RNAs become packaged genomes in the viral particles. *Virology* 454:455:362–370. <https://doi.org/10.1016/j.virol.2014.01.019>.
 34. Lu K, Heng X, Summers MF. 2011. Structural determinants and mechanism of HIV-1 genome packaging. *J Mol Biol* 410:609–633. <https://doi.org/10.1016/j.jmb.2011.04.029>.
 35. Kaddis Maldonado RJ, Parent LJ. 2016. Orchestrating the selection and packaging of genomic RNA by retroviruses: an ensemble of viral and host factors. *Viruses* 8:E257.
 36. Telesnitsky A, Wolin SL. 2016. The host RNAs in retroviral particles. *Viruses* 8:E235. <https://doi.org/10.3390/v8080235>.
 37. Leblanc J, Weil J, Beemon K. 2013. Posttranscriptional regulation of retroviral gene expression: primary RNA transcripts play three roles as pre-mRNA, mRNA, and genomic RNA. *Wiley Interdiscip Rev RNA* 4:567–580. <https://doi.org/10.1002/wrna.1179>.
 38. Lingappa JR, Reed JC, Tanaka M, Chutiraka K, Robinson BA. 2014. How HIV-1 Gag assembles in cells: putting together pieces of the puzzle. *Virus Res* 193:89–107. <https://doi.org/10.1016/j.virusres.2014.07.001>.
 39. Chen J, Grunwald D, Sardo L, Galli A, Plisov S, Nikolaitchik OA, Chen D, Lockett S, Larson DR, Pathak VK, Hu W-S. 2014. Cytoplasmic HIV-1 RNA is mainly transported by diffusion in the presence or absence of Gag protein. *Proc Natl Acad Sci U S A* 111:E5205–E5213. <https://doi.org/10.1073/pnas.1413169111>.
 40. Sardo L, Hatch SC, Chen J, Nikolaitchik O, Burdick RC, Chen D, Westlake CJ, Lockett S, Pathak VK, Hu W-S. 2015. Dynamics of HIV-1 RNA near the plasma membrane during virus assembly. *J Virol* 89:10832–10840. <https://doi.org/10.1128/JVI.01146-15>.
 41. Perez-Caballero D, Hatzioannou T, Martin-Serrano J, Bieniasz PD. 2004. Human immunodeficiency virus type 1 matrix inhibits and confers cooperativity on gag precursor-membrane interactions. *J Virol* 78: 9560–9563. <https://doi.org/10.1128/JVI.78.17.9560-9563.2004>.
 42. Hatzioannou T, Martin-Serrano J, Zang T, Bieniasz PD. 2005. Matrix-induced inhibition of membrane binding contributes to human immunodeficiency virus type 1 particle assembly defects in murine cells. *J Virol* 79:15586–15589. <https://doi.org/10.1128/JVI.79.24.15586-15589.2005>.
 43. Yadav SS, Wilson SJ, Bieniasz PD. 2012. A facile quantitative assay for viral particle genesis reveals cooperativity in virion assembly and saturation of an antiviral protein. *Virology* 429:155–162. <https://doi.org/10.1016/j.virol.2012.04.008>.
 44. Paillart JC, Göttlinger HG. 1999. Opposing effects of human immunodeficiency virus type 1 matrix mutations support a myristyl switch model of gag membrane targeting. *J Virol* 73:2604–2612.
 45. Hermidia-Matsumoto L, Resh MD. 1999. Human immunodeficiency virus type 1 protease triggers a myristoyl switch that modulates membrane binding of Pr55(gag) and p17MA. *J Virol* 73:1902–1908.
 46. Chen J, Nikolaitchik O, Singh J, Wright A, Bencsics CE, Coffin JM, Ni N, Lockett S, Pathak VK, Hu W-S. 2009. High efficiency of HIV-1 genomic RNA packaging and heterozygote formation revealed by single virion analysis. *Proc Natl Acad Sci U S A* 106:13535–13540. <https://doi.org/10.1073/pnas.0906822106>.
 47. Moore MD, Nikolaitchik OA, Chen J, Hammarkjöld M-L, Rekosh D, Hu W-S. 2009. Probing the HIV-1 genomic RNA trafficking pathway and dimerization by genetic recombination and single virion analyses. *PLoS Pathog* 5:e1000627. <https://doi.org/10.1371/journal.ppat.1000627>.
 48. Nikolaitchik OA, Dilley KA, Fu W, Gorelick RJ, Tai S-HS, Soheilian F, Ptak RG, Nagashima K, Pathak VK, Hu W-S. 2013. Dimeric RNA recognition regulates HIV-1 genome packaging. *PLoS Pathog* 9:e1003249. <https://doi.org/10.1371/journal.ppat.1003249>.
 49. Houzet L, Paillart JC, Smagulova F, Maurel S, Morichaud Z, Marquet R, Mougel M. 2007. HIV controls the selective packaging of genomic, spliced viral and cellular RNAs into virions through different mechanisms. *Nucleic Acids Res* 35:2695–2704. <https://doi.org/10.1093/nar/gkm153>.
 50. Lever A, Gottlinger H, Haseltine W, Sodroski J. 1989. Identification of a sequence required for efficient packaging of human immunodeficiency virus type 1 RNA into virions. *J Virol* 63:4085–4087.
 51. Kutluay SB, Zang T, Blanco-Melo D, Powell C, Jannain D, Errando M, Bieniasz PD. 2014. Global changes in the RNA binding specificity of HIV-1 gag regulate virion genesis. *Cell* 159:1096–1109. <https://doi.org/10.1016/j.cell.2014.09.057>.
 52. Keane SC, Heng X, Lu K, Kharytonchyk S, Ramakrishnan V, Carter G, Barton S, Hosie A, Florwick A, Santos J, Bolden NC, McCowin S, Case DA, Johnson BA, Salemi M, Telesnitsky A, Summers MF. 2015. Structure of the HIV-1 RNA packaging signal. *Science* 348:917–921. <https://doi.org/10.1126/science.aaa9266>.
 53. Cockrell AS, van Praag H, Santistevan N, Ma H, Kafri T. 2011. The HIV-1 Rev/RRE system is required for HIV-1 5' UTR cis elements to augment encapsidation of heterologous RNA into HIV-1 viral particles. *Retrovirology* 8:51. <https://doi.org/10.1186/1742-4690-8-51>.
 54. Brandt S, Blissenbach M, Grewe B, Konietzny R, Grunwald T, Überla K. 2007. Rev proteins of human and simian immunodeficiency virus enhance RNA encapsidation. *PLoS Pathog* 3:e54. <https://doi.org/10.1371/journal.ppat.0030054>.
 55. Pollard VW, Malim MH. 1998. The HIV-1 Rev protein. *Annu Rev Microbiol* 52:491–532. <https://doi.org/10.1146/annurev.micro.52.1.491>.
 56. Fernandes J, Jayaraman B, Frankel A. 2012. The HIV-1 Rev response element. *RNA Biol* 9:6–11. <https://doi.org/10.4161/rna.9.1.18178>.
 57. Rausch JW, Le Grice SFJ. 2015. HIV Rev assembly on the Rev response element (RRE): a structural perspective. *Viruses* 7:3053–3075. <https://doi.org/10.3390/v7062760>.
 58. Ferrer M, Clercé C, Chamontin C, Basyuk E, Lainé S, Hottin J, Bertrand E, Margeat E, Mougel M. 2016. Imaging HIV-1 RNA dimerization in cells by

- multicolor super-resolution and fluctuation microscopies. *Nucleic Acids Res* 44:7922–7934. <https://doi.org/10.1093/nar/gkw511>.
59. Chen J, Rahman SA, Nikolaitchik OA, Grunwald D, Sardo L, Burdick RC, Plisov S, Liang E, Tai S, Pathak VK, Hu W-S. 2016. HIV-1 RNA genome dimerizes on the plasma membrane in the presence of Gag protein. *Proc Natl Acad Sci U S A* 113:E201–E208. <https://doi.org/10.1073/pnas.1518572113>.
 60. Ivanchenko S, Godinez WJ, Lampe M, Kräusslich H-G, Eils R, Rohr K, Bräuchle C, Müller B, Lamb DC. 2009. Dynamics of HIV-1 assembly and release. *PLoS Pathog* 5:e1000652. <https://doi.org/10.1371/journal.ppat.1000652>.
 61. Ku P-I, Miller AK, Ballew J, Sandrin V, Adler FR, Saffarian S. 2013. Identification of pauses during formation of HIV-1 virus like particles. *Biophys J* 105:2262–2272. <https://doi.org/10.1016/j.bpj.2013.09.047>.
 62. Onafuwu-Nuga AA, Telesnitsky A, King SR. 2006. 7SL RNA, but not the 54-kd signal recognition particle protein, is an abundant component of both infectious HIV-1 and minimal virus-like particles. *RNA* 12:542–546. <https://doi.org/10.1261/rna.2306306>.
 63. Didierlaurent L, Racine PJ, Houzet L, Chamontin C, Berkhouit B, Mougel M. 2011. Role of HIV-1 RNA and protein determinants for the selective packaging of spliced and unspliced viral RNA and host U6 and 7SL RNA in virus particles. *Nucleic Acids Res* 39:8915–8927. <https://doi.org/10.1093/nar/gkr577>.
 64. Chukkapalli V, Hogue IB, Boyko V, Hu W-S, Ono A. 2008. Interaction between the human immunodeficiency virus type 1 Gag matrix domain and phosphatidylinositol-(4,5)-bisphosphate is essential for efficient gag membrane binding. *J Virol* 82:2405–2417. <https://doi.org/10.1128/JVI.01614-07>.
 65. Chukkapalli V, Oh SJ, Ono A. 2010. Opposing mechanisms involving RNA and lipids regulate HIV-1 Gag membrane binding through the highly basic region of the matrix domain. *Proc Natl Acad Sci U S A* 107:1600–1605. <https://doi.org/10.1073/pnas.0908661107>.
 66. Gheysen D, Jacobs E, de Foresta F, Thiriart C, Francotte M, Thines D, De Wilde M. 1989. Assembly and release of HIV-1 precursor Pr55gag virus-like particles from recombinant baculovirus-infected insect cells. *Cell* 59:103–112. [https://doi.org/10.1016/0092-8674\(89\)90873-8](https://doi.org/10.1016/0092-8674(89)90873-8).
 67. Smith AJ, Cho MI, Hammarskjöld ML, Rekosh D. 1990. Human immunodeficiency virus type 1 Pr55gag and Pr160gag-pol expressed from a simian virus 40 late replacement vector are efficiently processed and assembled into viruslike particles. *J Virol* 64:2743–2750.
 68. Wills JW, Craven RC. 1991. Form, function, and use of retroviral gag proteins. *AIDS (Lond, Engl)* 5:639–654. <https://doi.org/10.1097/00002030-199106000-00002>.
 69. Zhang Y, Qian H, Love Z, Barklis E. 1998. Analysis of the assembly function of the human immunodeficiency virus type 1 gag protein nucleocapsid domain. *J Virol* 72:1782–1789.
 70. Accola MA, Strack B, Göttlinger HG. 2000. Efficient particle production by minimal Gag constructs which retain the carboxy-terminal domain of human immunodeficiency virus type 1 capsid-p2 and a late assembly domain. *J Virol* 74:5395–5402. <https://doi.org/10.1128/JVI.74.12.5395-5402.2000>.
 71. Muriaux D, Costes S, Nagashima K, Mirro J, Cho E, Lockett S, Rein A. 2004. Role of murine leukemia virus nucleocapsid protein in virus assembly. *J Virol* 78:12378–12385. <https://doi.org/10.1128/JVI.78.22.12378-12385.2004>.
 72. Patel N, Dykeman EC, Coutts RHA, Lomonosoff GP, Rowlands DJ, Phillips SEV, Ranson N, Twarock R, Tuma R, Stockley PG. 2015. Revealing the density of encoded functions in a viral RNA. *Proc Natl Acad Sci U S A* 112:2227–2232. <https://doi.org/10.1073/pnas.1420812112>.
 73. Rolfsson Ó, Middleton S, Manfield IW, White SJ, Fan B, Vaughan R, Ranson NA, Dykeman E, Twarock R, Ford J, Kao CC, Stockley PG. 2016. Direct evidence for packaging signal-mediated assembly of bacteriophage MS2. *J Mol Biol* 428:431–448. <https://doi.org/10.1016/j.jmb.2015.11.014>.
 74. Stockley PG, White SJ, Dykeman E, Manfield I, Rolfsson O, Patel N, Bingham R, Barker A, Wroblewski E, Chandler-Bostock R, Weiβ EU, Ranson NA, Tuma R, Twarock R. 2016. Bacteriophage MS2 genomic RNA encodes an assembly instruction manual for its capsid. *Bacteriophage* 6:e1157666. <https://doi.org/10.1080/21597081.2016.1157666>.
 75. Swanson CM, Puffer BA, Ahmad KM, Doms RW, Malim MH. 2004. Retroviral mRNA nuclear export elements regulate protein function and virion assembly. *EMBO J* 23:2632–2640. <https://doi.org/10.1038/sj.emboj.7600270>.
 76. Swanson CM, Malim MH. 2006. Retrovirus RNA trafficking: from chromatin to invasive genomes. *Traffic* 7:1440–1450. <https://doi.org/10.1111/j.1600-0854.2006.00488.x>.
 77. Jin J, Sturgeon T, Chen C, Watkins SC, Weisz OA, Montelaro RC. 2007. Distinct intracellular trafficking of equine infectious anemia virus and human immunodeficiency virus type 1 Gag during viral assembly and budding revealed by bimolecular fluorescence complementation assays. *J Virol* 81:11226–11235. <https://doi.org/10.1128/JVI.00431-07>.
 78. Jin J, Sturgeon T, Weisz OA, Mothes W, Montelaro RC. 2009. HIV-1 matrix dependent membrane targeting is regulated by Gag mRNA trafficking. *PLoS One* 4:e6551. <https://doi.org/10.1371/journal.pone.0006551>.
 79. Sherer NM, Swanson CM, Papaioannou S, Malim MH. 2009. Matrix mediates the functional link between human immunodeficiency virus type 1 RNA nuclear export elements and the assembly competency of Gag in murine cells. *J Virol* 83:8525–8535. <https://doi.org/10.1128/JVI.00699-09>.
 80. Diaz-Griffero F, Taube R, Muehlbauer SM, Brojatsch J. 2008. Efficient production of HIV-1 viral-like particles in mouse cells. *Biochem Biophys Res Commun* 368:463–469. <https://doi.org/10.1016/j.bbrc.2007.12.195>.
 81. Pocock GM, Becker JT, Swanson CM, Ahlquist P, Sherer NM. 2016. HIV-1 and M-PMV RNA nuclear export elements program viral genomes for distinct cytoplasmic trafficking behaviors. *PLoS Pathog* 12:e1005565. <https://doi.org/10.1371/journal.ppat.1005565>.
 82. Schwartz S, Campbell M, Nasioulas G, Harrison J, Felber BK, Pavlakis GN. 1992. Mutational inactivation of an inhibitory sequence in human immunodeficiency virus type 1 results in Rev-independent gag expression. *J Virol* 66:7176–7182.
 83. Hermida-Matsumoto L, Resh MD. 2000. Localization of human immunodeficiency virus type 1 Gag and Env at the plasma membrane by confocal imaging. *J Virol* 74:8670–8679. <https://doi.org/10.1128/JVI.74.18.8670-8679.2000>.
 84. Nikolaitchik O, Rhodes TD, Ott D, Hu W-S. 2006. Effects of mutations in the human immunodeficiency virus type 1 Gag gene on RNA packaging and recombination. *J Virol* 80:4691–4697. <https://doi.org/10.1128/JVI.80.10.4691-4697.2006>.
 85. Buck CB, Shen X, Egan MA, Pierson TC, Walker CM, Siliciano RF. 2001. The human immunodeficiency virus type 1 gag gene encodes an internal ribosome entry site. *J Virol* 75:181–191. <https://doi.org/10.1128/JVI.75.1.181-191.2001>.
 86. Poon DTK, Chertova EN, Ott DE. 2002. Human immunodeficiency virus type 1 preferentially encapsidates genomic RNAs that encode Pr55Gag: functional linkage between translation and RNA packaging. *Virology* 293:368–378. <https://doi.org/10.1006/viro.2001.1283>.
 87. Sigal CT, Zhou W, Buser CA, McLaughlin S, Resh MD. 1994. Amino-terminal basic residues of Src mediate membrane binding through electrostatic interaction with acidic phospholipids. *Proc Natl Acad Sci U S A* 91:12253–12257. <https://doi.org/10.1073/pnas.91.25.12253>.
 88. Yang J, Bogerd HP, Wang PJ, Page DC, Cullen BR. 2001. Two closely related human nuclear export factors utilize entirely distinct export pathways. *Mol Cell* 8:397–406. [https://doi.org/10.1016/S1097-2765\(01\)00303-3](https://doi.org/10.1016/S1097-2765(01)00303-3).
 89. Wiegand HL, Coburn GA, Zeng Y, Kang Y, Bogerd HP, Cullen BR. 2002. Formation of Tap/NXT1 heterodimers activates Tap-dependent nuclear mRNA export by enhancing recruitment to nuclear pore complexes. *Mol Cell Biol* 22:245–256. <https://doi.org/10.1128/MCB.22.1.245-256.2002>.
 90. Bunce MW, Bergendahl K, Anderson RA. 2006. Nuclear PI(4,5)P₂: a new place for an old signal. *Biochim Biophys Acta* 1761:560–569. <https://doi.org/10.1016/j.bbaply.2006.03.002>.
 91. Anderson EC, Lever AML. 2006. Human immunodeficiency virus type 1 Gag polyprotein modulates its own translation. *J Virol* 80:10478–10486. <https://doi.org/10.1128/JVI.02596-05>.
 92. Haucke V. 2005. Phosphoinositide regulation of clathrin-mediated endocytosis. *Biochem Soc Trans* 33:1285–1289. <https://doi.org/10.1042/BST0331285>.
 93. Ott DE, Coren LV, Kane BP, Busch LK, Johnson DG, Sowder RC, Chertova EN, Arthur LO, Henderson LE. 1996. Cytoskeletal proteins inside human immunodeficiency virus type 1 virions. *J Virol* 70:7734–7743.
 94. Jolly C, Kashefi K, Hollinshead M, Sattentau QJ. 2004. HIV-1 cell to cell transfer across an Env-induced, actin-dependent synapse. *J Exp Med* 199:283–293. <https://doi.org/10.1084/jem.20030648>.
 95. Sasaki H, Ozaki H, Karaki H, Nonomura Y. 2004. Actin filaments play an essential role for transport of nascent HIV-1 proteins in host cells.

- Biochem Biophys Res Commun 316:588–593. <https://doi.org/10.1016/j.bbrc.2004.02.088>.
96. Cooper J, Liu L, Woodruff EA, Taylor HE, Goodwin JS, D'Aquila RT, Spearman P, Hildreth JEK, Dong X. 2011. Filamin A protein interacts with human immunodeficiency virus type 1 Gag protein and contributes to productive particle assembly. *J Biol Chem* 286:28498–28510. <https://doi.org/10.1074/jbc.M111.239053>.
 97. Wen X, Ding L, Wang J-J, Qi M, Hammonds J, Chu H, Chen X, Hunter E, Spearman P. 2014. ROCK1 and LIM kinase modulate retrovirus particle release and cell-cell transmission events. *J Virol* 88:6906–6921. <https://doi.org/10.1128/JVI.00023-14>.
 98. Thomas A, Mariani-Floderer C, López-Huertas MR, Gros N, Hamard-Péron E, Favard C, Ohlmann T, Alcamí J, Muriaux D. 2015. Involvement of the Rac1-IRSp53-Wave2-Arp2/3 signaling pathway in HIV-1 Gag particle release in CD4 T cells. *J Virol* 89:8162–8181. <https://doi.org/10.1128/JVI.00469-15>.
 99. Riedl J, Crevenna AH, Kessenbrock K, Yu JH, Neukirchen D, Bista M, Bradke F, Jenne D, Holak TA, Werb Z, Sixt M, Wedlich-Soldner R. 2008. Lifeact: a versatile marker to visualize F-actin. *Nat Methods* 5:605–607. <https://doi.org/10.1038/nmeth.1220>.
 100. Bray M, Prasad S, Dubay JW, Hunter E, Jeang KT, Rekosh D, Hammar-skjöld ML. 1994. A small element from the Mason-Pfizer monkey virus genome makes human immunodeficiency virus type 1 expression and replication Rev-independent. *Proc Natl Acad Sci U S A* 91:1256–1260. <https://doi.org/10.1073/pnas.91.4.1256>.
 101. Wodrich H, Schambach A, Kräusslich HG. 2000. Multiple copies of the Mason-Pfizer monkey virus constitutive RNA transport element lead to enhanced HIV-1 Gag expression in a context-dependent manner. *Nucleic Acids Res* 28:901–910. <https://doi.org/10.1093/nar/28.4.901>.
 102. Dooher JE, Lingappa JR. 2004. Conservation of a stepwise, energy-sensitive pathway involving HP68 for assembly of primate lentivirus capsids in cells. *J Virol* 78:1645–1656. <https://doi.org/10.1128/JVI.78.4.1645-1656.2004>.
 103. Kutluay SB, Bieniasz PD. 2010. Analysis of the initiating events in HIV-1 particle assembly and genome packaging. *PLoS Pathog* 6:e1001200. <https://doi.org/10.1371/journal.ppat.1001200>.
 104. Robinson BA, Reed JC, Geary CD, Swain JV, Lingappa JR. 2014. A temporospatial map that defines specific steps at which critical surfaces in the Gag MA and CA domains act during immature HIV-1 capsid assembly in cells. *J Virol* 88:5718–5741. <https://doi.org/10.1128/JVI.03609-13>.
 105. Ma H, Cockrell A, Bash R, VanDyke T, Kafri T. 2005. 822. A Rev/RRE dependent packaging system for MLV based vectors raises biosafety concerns. *Mol Ther* 11:S320.
 106. Gewe B, Ehrhardt K, Hoffmann B, Blissenbach M, Brandt S, Überla K. 2012. The HIV-1 Rev protein enhances encapsidation of unspliced and spliced, RRE-containing lentiviral vector RNA. *PLoS One* 7:e48688. <https://doi.org/10.1371/journal.pone.0048688>.
 107. Anderson P, Kedersha N, Ivanov P. 2015. Stress granules, P-bodies and cancer. *Biochim Biophys Acta* 1849:861–870. <https://doi.org/10.1016/j.bbagr.2014.11.009>.
 108. Brangwynne CP. 2013. Phase transitions and size scaling of membraneless organelles. *J Cell Biol* 203:875–881. <https://doi.org/10.1083/jcb.201308087>.
 109. Zimmerman C, Klein KC, Kiser PK, Singh AR, Firestein BL, Riba SC, Lingappa JR. 2002. Identification of a host protein essential for assembly of immature HIV-1 capsids. *Nature* 415:88–92. <https://doi.org/10.1038/415088a>.
 110. Yedavalli VSRK, Neuveut C, Chi Y-H, Kleiman L, Jeang K-T. 2004. Requirement of DDX3 DEAD box RNA helicase for HIV-1 Rev-RRE export function. *Cell* 119:381–392. <https://doi.org/10.1016/j.cell.2004.09.029>.
 111. Cochrane AW, McNally MT, Mouland AJ. 2006. The retrovirus RNA trafficking granule: from birth to maturity. *Retrovirology* 3:18. <https://doi.org/10.1128/JVI.1742-4690-3-18>.
 112. Naji S, Ambrus G, Čimermančič P, Reyes JR, Johnson JR, Filbrandt R, Huber MD, Vesely P, Krogan NJ, Yates JR, Saphire AC, Gerace L. 2012. Host cell interactome of HIV-1 Rev includes RNA helicases involved in multiple facets of virus production. *Mol Cell Proteomics* 11: M111.015313. <https://doi.org/10.1074/mcp.M111.015313>.
 113. Reed JC, Molter B, Geary CD, McNevin J, McElrath J, Giri S, Klein KC, Lingappa JR. 2012. HIV-1 Gag co-opts a cellular complex containing DDX6, a helicase that facilitates capsid assembly. *J Cell Biol* 198: 439–456. <https://doi.org/10.1083/jcb.201111012>.
 114. Chatel-Chaix L, Clément J-F, Martel C, Bérilault V, Gatignol A, DesGroveilliers L, Mouland AJ. 2004. Identification of Staufen in the human immunodeficiency virus type 1 Gag ribonucleoprotein complex and a role in generating infectious viral particles. *Mol Cell Biol* 24:2637–2648. <https://doi.org/10.1128/MCB.24.7.2637-2648.2004>.
 115. Swanson CM, Sherer NM, Malim MH. 2010. SRp40 and SRp55 promote the translation of unspliced human immunodeficiency virus type 1 RNA. *J Virol* 84:6748–6759. <https://doi.org/10.1128/JVI.02526-09>.
 116. Mouland AJ, Xu H, Cui H, Krueger W, Munro TP, Prasol M, Mercier J, Rekosh D, Smith R, Barbarese E, Cohen EA, Carson JH. 2001. RNA trafficking signals in human immunodeficiency virus type 1. *Mol Cell Biol* 21:2133–2143. <https://doi.org/10.1128/MCB.21.6.2133-2143.2001>.
 117. Lévesque K, Halvorsen M, Abrahamyan L, Chatel-Chaix L, Poupon V, Gordon H, DesGroveilliers L, Gatignol A, Mouland AJ. 2006. Trafficking of HIV-1 RNA is mediated by heterogeneous nuclear ribonucleoprotein A2 expression and impacts on viral assembly. *Traffic* 7:1177–1193. <https://doi.org/10.1111/j.1600-0854.2006.00461.x>.
 118. Boeras I, Song Z, Moran A, Franklin J, Brown WC, Johnson M, Boris-Lawrie K, Heng X. 2016. DHX9/RHA binding to the PBS-segment of the genomic RNA during HIV-1 assembly bolsters virion infectivity. *J Mol Biol* 428:2418–2429. <https://doi.org/10.1016/j.jmb.2016.04.011>.
 119. Bolinger C, Boris-Lawrie K. 2009. Mechanisms employed by retroviruses to exploit host factors for translational control of a complicated proteome. *Retrovirology* 6:8. <https://doi.org/10.1186/1742-4690-6-8>.
 120. Lécuyer E, Yoshida H, Parthasarathy N, Alm C, Babak T, Cerovina T, Hughes TR, Tomancak P, Krause HM. 2007. Global analysis of mRNA localization reveals a prominent role in organizing cellular architecture and function. *Cell* 131:174–187. <https://doi.org/10.1016/j.cell.2007.08.003>.
 121. Sinnamom JR, Czaplinski K. 2011. mRNA trafficking and local translation: the Yin and Yang of regulating mRNA localization in neurons. *Acta Biochim Biophys Sin* 43:663–670. <https://doi.org/10.1093/abbs/gmr058>.
 122. Herrera-Carrillo E, Berkhouit B. 2015. Bone marrow gene therapy for HIV/AIDS. *Viruses* 7:3910–3936. <https://doi.org/10.3390/v7072804>.
 123. Lloyd RE. 2013. Regulation of stress granules and P-bodies during RNA virus infection. *Wiley Interdiscip Rev RNA* 4:317–331. <https://doi.org/10.1002/wrna.1162>.
 124. Bosse JB, Hogue IB, Feric M, Thibierge SY, Sodeik B, Brangwynne CP, Enquist LW. 2015. Remodeling nuclear architecture allows efficient transport of herpesvirus capsids by diffusion. *Proc Natl Acad Sci U S A* 112:E5725–E5733. <https://doi.org/10.1073/pnas.1513876112>.
 125. Shukla S, Parker R. 2016. Hypo- and hyper-assembly diseases of RNA-protein complexes. *Trends Mol Med* 22:615–628. <https://doi.org/10.1016/j.molmed.2016.05.005>.
 126. Adachi A, Gendelman HE, Koenig S, Folks T, Willey R, Rabson A, Martin MA. 1986. Production of acquired immunodeficiency syndrome-associated retrovirus in human and nonhuman cells transfected with an infectious molecular clone. *J Virol* 59:284–291.
 127. Connor RL, Chen BK, Choe S, Landau NR. 1995. Vpr is required for efficient replication of human immunodeficiency virus type-1 in mono-nuclear phagocytes. *Virology* 206:935–944. <https://doi.org/10.1006/viro.1995.1016>.
 128. Phalora PK, Sherer NM, Wolinsky SM, Swanson CM, Malim MH. 2012. HIV-1 replication and APOBEC3 antiviral activity are not regulated by P bodies. *J Virol* 86:11712–11724. <https://doi.org/10.1128/JVI.00595-12>.
 129. Subach OM, Cranfill PJ, Davidson MW, Verkushava VV. 2011. An enhanced monomeric blue fluorescent protein with the high chemical stability of the chromophore. *PLoS One* 6:e28674. <https://doi.org/10.1371/journal.pone.0028674>.
 130. Femino AM, Fay FS, Fogarty K, Singer RH. 1998. Visualization of single RNA transcripts in situ. *Science* 280:585–590. <https://doi.org/10.1126/science.280.5363.585>.
 131. Kalderon D, Roberts BL, Richardson WD, Smith AE. 1984. A short amino acid sequence able to specify nuclear location. *Cell* 39:499–509. [https://doi.org/10.1016/0092-8674\(84\)90457-4](https://doi.org/10.1016/0092-8674(84)90457-4).
 132. Sheehy AM, Gaddis NC, Choi JD, Malim MH. 2002. Isolation of a human gene that inhibits HIV-1 infection and is suppressed by the viral Vif protein. *Nature* 418:646–650. <https://doi.org/10.1038/nature00939>.
 133. Sherer NM, Swanson CM, Hué S, Roberts RG, Bergeron JRC, Malim MH. 2011. Evolution of a species-specific determinant within human CRM1 that regulates the post-transcriptional phases of HIV-1 replication. *PLoS Pathog* 7:e1002395. <https://doi.org/10.1371/journal.ppat.1002395>.
 134. Aligeti M, Behrens RT, Pocock GM, Schindelin J, Dietz C, Eliceiri KW, Swanson CM, Malim MH, Ahlquist P, Sherer NM. 2014. Cooperativity among Rev-associated nuclear export signals regulates HIV-1 gene

- expression and is a determinant of virus species tropism. *J Virol* 88: 14207–14221. <https://doi.org/10.1128/JVI.01897-14>.
135. Chesebro B, Wehrly K, Nishio J, Perryman S. 1992. Macrophage-tropic human immunodeficiency virus isolates from different patients exhibit unusual V3 envelope sequence homogeneity in comparison with T-cell-tropic isolates: definition of critical amino acids involved in cell tropism. *J Virol* 66:6547–6554.
136. Schindelin J, Arganda-Carreras I, Frise E, Kaynig V, Longair M, Pietzsch T, Preibisch S, Rueden C, Saalfeld S, Schmid B, Tinevez J-Y, White DJ, Hartenstein V, Eliceiri K, Tomancak P, Cardona A. 2012. Fiji: an open-source platform for biological-image analysis. *Nat Methods* 9:676–682. <https://doi.org/10.1038/nmeth.2019>.
137. Garcia-Miranda P, Becker JT, Benner BE, Blume A, Sherer NM, Butcher SE. 2016. Stability of HIV frameshift site RNA correlates with frameshift efficiency and decreased virus infectivity. *J Virol* 90:6906–6917. <https://doi.org/10.1128/JVI.00149-16>.